Isotopic characterisation of mineralised skarn in Pernatty Lagoon

Thesis submitted in accordance with the requirements of the University of Adelaide for an Honours Degree in Geology

Nestor Wyra

November 2017

THE UNIVERSITY of ADELAIDE

STABLE AND RADIOGENIC ISOTOPE CHARACTERISATION OF SKARN MINERALISATION IN PERNATTY LAGOON

ISOTOPIC CHARACTERISATION OF MINERALISED SKARN IN PERNATTY LAGOON

ABSTRACT

The Pernatty Lagoon skarn deposit is located in the Stuart Shelf within the Gawler Craton, approximately 50km South of Carapateena. Investigation into the isotopic signatures of mineralised skarns in Pernatty Lagoon will identify the fluid source of mineralisation and aid in mineralogical exploration in the Olympic Dam province. The age of the skarn is proposed to be the product of fluids from the Gawler Range Volcanics or Hiltaba Intrusive Suite interacting with metasediments of the Wallaroo Group at 1577±7 Ma. Mineralisation in the skarn is dominated by chalcopyrite, galena and zinc. A large-scale alteration halo defines the region, and exemplifies a complex geological history involving many stages of fluid-rock interaction. Andradite garnet is highly abundant throughout the skarn alongside quartz and calcite veins, potassium-feldspar, chlorite, talc, and amphibole. In this study $\delta^{18}O$ and δD values were obtained from bulk rock samples in Pernatty Lagoon, yielding values ranging between 4.7 to 14.1 and -80.1 to -45.5, with averages of 10.6 and -61.7 respectively, and show mixing of magmatic water and metasediments.

εNd values were calculated from samples obtained from Pernatty Lagoon during this study, and were based on the inferred age of skarn formation, and yielded values ranging between -5.72 and -7.55 with a mean of -6.68. These values suggest the skarn and by association mineralisation was formed by evolved crustally derived fluids. Trace element data obtained from garnets in Pernatty Lagoon suggest the skarn forming fluid was acidic, saline, and likely of granitic origin. Stable and radiogenic isotope data, as well as trace element and REE data all strongly indicate that skarn mineralisation occurred under reduced, saline and acidic conditions due to the emplacement of the Hiltaba Intrusive Suite into Wallaroo Group metasediments. These findings are of significance as it confirms the Hiltaba Intrusive Suite to be the driving force of mineralisation in Pernatty Lagoon, and that Pernatty Lagoon mineralisation was independent of Olympic Dam.

KEYWORDS

Stable isotope, radiogenic isotope, skarn, Pernatty Lagoon, IOCG, REE. Trace element, fluid, Gawler Craton.

TABLE OF CONTENTS

LIST OF FIGURES AND TABLES

INTRODUCTION

Analysis of stable and radiogenic isotopes within mineralised and altered regions can be used to identify possible relationships between previous regions of mineralisation and distal signatures from other mineralisation events (Johnson and McCulloch, 1995). Geochemical and textural analysis of sulphide mineralisation within skarns in conjunction with isotopic data could infer the fluid source or sources of mineralisation within a system. Isotopic analysis has yet to be conducted on orebodies in Pernatty Lagoon, and therefore the significance of the relationship between isotopic signatures and mineralisation in this region is. The country rock as well as mineralisation itself contains isotopic signatures that reflect its geological history, including the composition of any fluids that percolated through and changed the chemistry of the bulk rock (Schlegel and Heinrich, 2015).

Pernatty Lagoon is located in the Stuart Shelf in the East Gawler Craton, South Australia (Figure 1), and is dominated skarn-garnets, formed by Moonta-Wallaroo group calcareous sediments reacting with percolating fluids after deposition in sedimentary basins in the primordial Gawler Craton. The skarn exists in well-defined beds ranging between 200 and 400m in thickness (Hand et al., 2007; Reid et al., 2011). The Hiltaba Intrusive Suite (HIS) was emplaced 1.6 Ga ago (Reid et al., 2011) and is thought to have been a factor in the mineralisation of the Eastern Gawler Craton. Therefore, it is considered a possible fluid source for the mineralisation found in Pernatty Lagoon.

This paper compares the isotopic signatures of stable and radiogenic isotopes to unaltered protolith in the drillhole 20610 (SAR8) in Pernatty Lagoon with the aim to determine the nature of fluid sources linked to skarn-associated mineralisation using stable isotope mass spectrometry, thermal ionisation mass (TIMS). Rare earth element (REE) and trace element content from garnets within the skarn will also be compared to isotopic and geochemical data using laser ablation inductively-coupled plasma-mass spectrometry (LA–ICP–MS) to determine a relationship between isotopic signatures, mineralisation and relative enrichment of REES and trace elements.

Figures 1a and 1b show the proximity of Pernatty Lagoon to the Punt Hill prospect. Investigations at Punt Hill have shown similarities in mineralogy and isotopic composition between Punt Hill and Pernatty Lagoon.

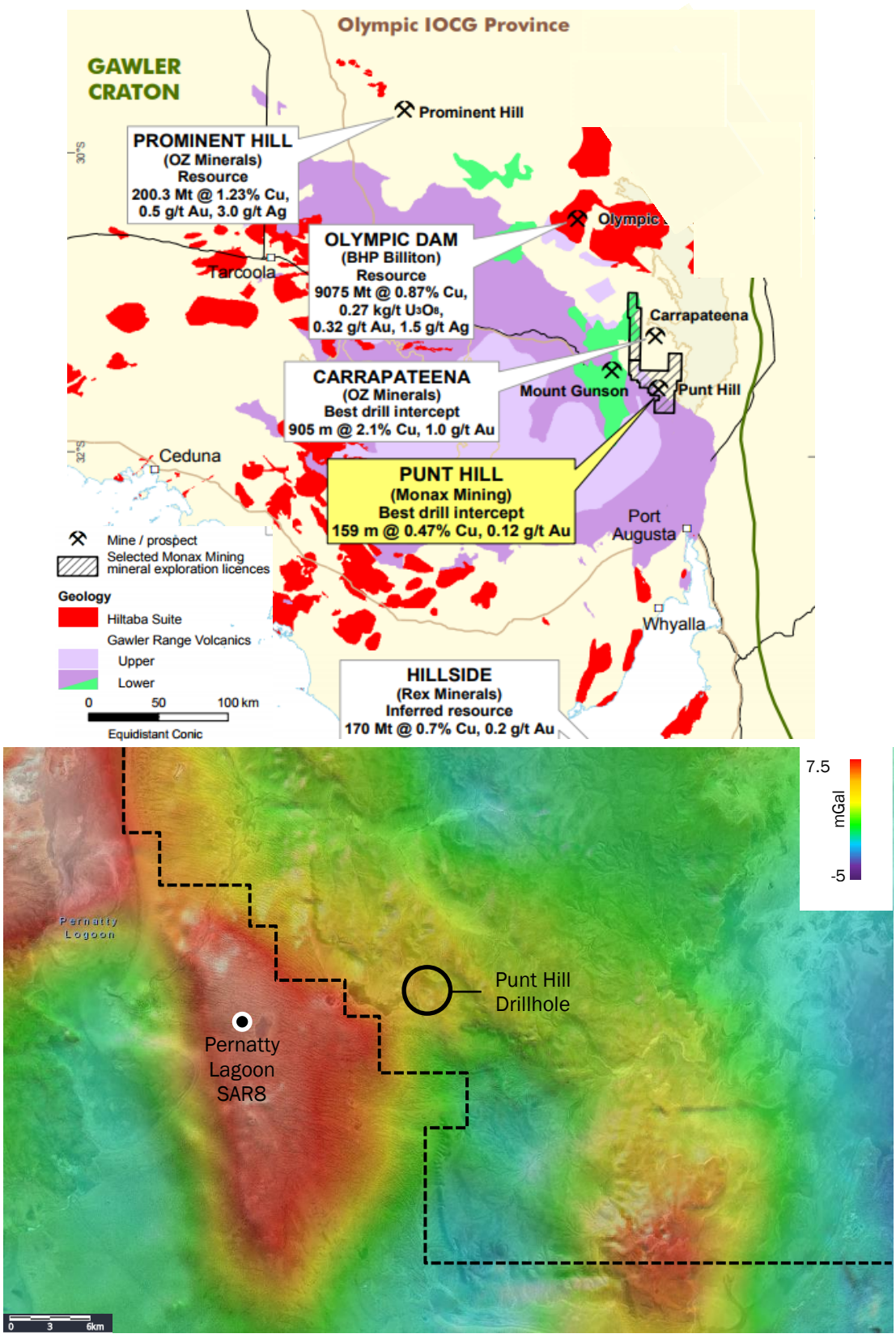

Figure 1: a) Geology of the Olympic IOCG Province in the Gawler Craton depicting the locations of various prospects. Figure 1: b) TMI and location of Pernatty Lagoon relative to Punt Hill and Figure 1a. Modified from (Reid et al., 2011).

GEOLOGICAL SETTING

Gawler Craton

The area of interest known as Pernatty Lagoon is situated on the Eastern side of the Gawler Craton on the Stuart shelf, and within the Olympic IOCG Province in South Australia. The basement of the Gawler Craton was formed in the late Archean as a result of ultramafic, mafic and felsic magmatism that was later metamorphosed during the Sleafordian Orogeny (2465–2410 Ma); (Hand et al., 2007). The many sedimentary basins that facilitate mineralisation in the Gawler Craton were formed by early rifting and emplacement of felsic and mafic igneous rocks approximately 2000 Ma (Skirrow et al., 2007). Short-lived episodes of crustal shortening caused melting of the Archean basement at approximately 1850 Ma forming the Donington granite suite (Hand et al., 2007).

Basinal deposition of sediments within the Gawler Craton is thought to have occurred between 1865 to 1740, during which the Wallaroo sedimentary group formed at approximately 1790–1740 Ma, and hosts mineralisation at Pernatty Lagoon. The Kimban Orogeny between 1730 and 1690 Ma ceased further sedimentary deposition. Continued tectonic evolution resulted in the arc-environment developing into a craton and formed the Gawler Range Volcanics (GRV) at 1595–1587 Ma (Hand et al., 2007).

Perhaps the most significant petrological and tectonic event to occur within the Gawler Craton is the emplacement of the Hiltaba Intrusive Suite (HIS) 1595–1570 Ma, which intrudes into the Wallaroo group and GRV and is believed to be synchronous with

large-scale IOCG Mineralisation throughout the Eastern Gawler Craton (Fabris et al., 2016; Hand et al., 2007; Nikolakopolous, 2013; Reid et al., 2011).

Adelaedian rocks of the Stuart shelf uncomformably overlie the Proterozoic basin and comprise of vesicular basalts, overlying the Donnington Suite, Wallaroo Group, GRV and HIS, sandy redbeds limestone, quartzite and sandstone (Reid et al., 2009; Reid et al., 2011)

Pernatty Lagoon

The mineralisation at Pernatty Lagoon is largely hosted in skarns, with predominantly abundant Cu–Zn–Pb mineralisation and lesser Au–and REE mineralisation throughout. The types of mineralisation and alteration in Pernatty Lagoon is incredibly similar to those of other sites in the Olympic IOCG Province (Ismail et al., 2014; Nikolakopolous, 2013). The drillhole of interest at Pernatty Lagoon is PRL21/SAR8, situated 120km north of Port Augusta. It contains strongly mineralised zones, as well as separate areas of comparatively little to no mineralisation as shown in Table 1 and Figure 2.

The mineralised zone within the analysed 968m core spanned a total of 120m and featured 3.2% Cu, 0.4% Pb and 1.3 % Zn as well as trace Ag and Au. Within that 120m mineralised section lies a particularly enriched intercept containing 2.6% Cu. The interval of mineralised skarn in SAR8 is approximately 200–300m thick situated between the overlying GRV and underlying Donnington suite.

The formation of garnet-diopside rocks from Punt Hill was dated using Sm–Nd isochrons indicates an age of approximately 1577$\pm$7 Ma (Reid et al., 2011) at Punt hill, which is inferred to be of same age as the garnet-skarns found at Pernatty Lagoon due to

their proximity. Furthermore this age range conforms with many other studies to infer the time at which mineralisation at Olympic Dam formed (Ciobanu et al., 2013; Fabris et al., 2016; Nikolakopolous, 2013; Skirrow et al., 2007). The underlying Donnington Suite formed at 1800 Ma, inferring a lack of genetic correlation between the formation of the mineralised skarn, and emplacement of the Donnington Suite. Despite the temporal difference between the formation of the two suites, the older Donnington Suite may provide structural and lithological traps for mineralisation such as in Carapateena, (Conor et al., 2010; Nikolakopolous, 2013), situated approximately 50km north-west of Pernatty Lagoon (Figure 1).

Table 1: Cu, Zn, and Pb concentrations in interval of interest within SAR8, Pernatty Lagoon.

Depth (m)	Sample ID	Cu (ppm)	Zn (ppm)	Pb (ppm)
906.3	65	24	38	5
970.6	71	12	258	45
1029.3	77	1394	142	169
1039.1	78	701	114	49
1050.1	79	1164	882	176
1089	82	130	120	49
1099.2	83	2451	722	64
1108.4	84	334	355	60
1119.25	85	552	3373	1140
1130.3	86	6417	247	80
1138.8	87	1347	807	406
1148.7	88	17913	278	84
1160.5	89	52	299	137
1170.85	90	388	163	31
1179.8	91	750	2894	1062
1201	93	798	2571	1394
1269.3	99	12	546	53

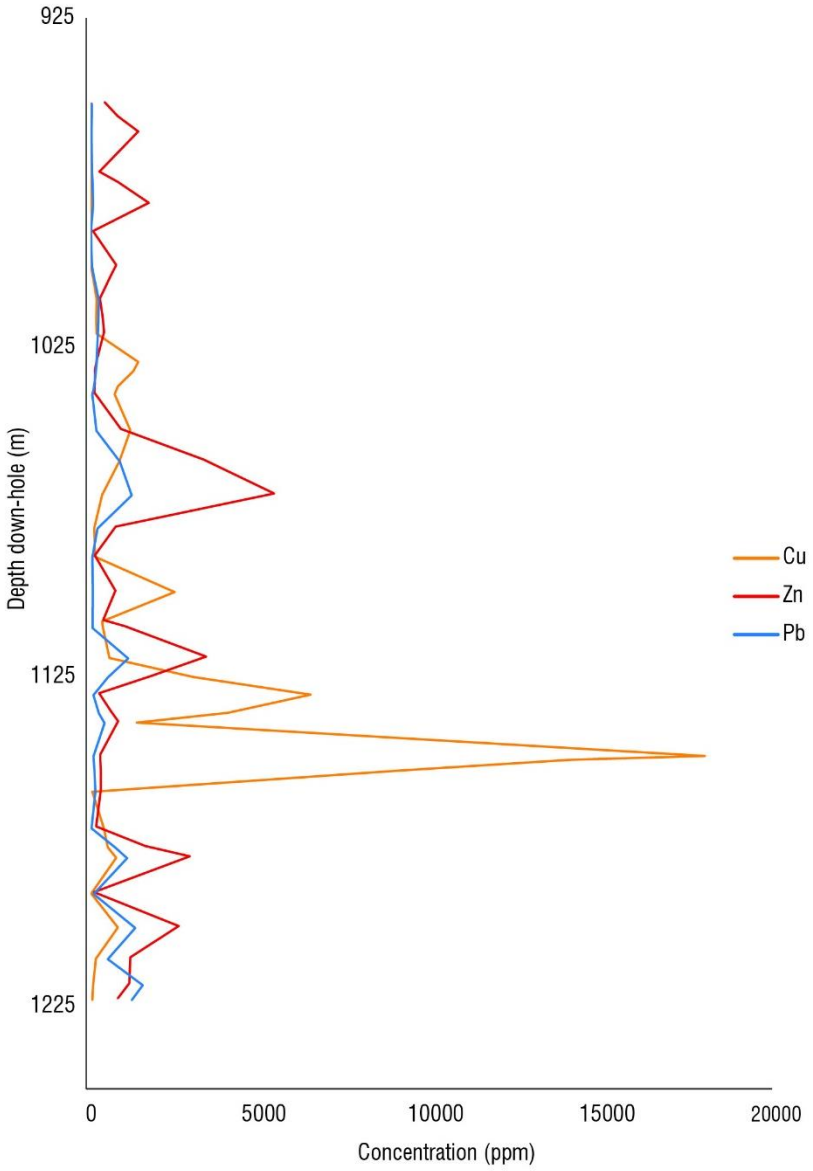

Figure 2: Cu, Pb and Zn content downhole in SAR8. The extent of geochemical data displayed in the figure describes the analysed interval in this study.

METHODS

Optical petrography and mineralogical study were performed on face slices and whole cores of SAR8 from Pernatty Lagoon. A total of forty samples were taken representing calcic-silicate skarns, metasediments, mineralised, and segments of the core, with a sample taken at the least mineralised and altered location from the same stratigraphic unit within the core.

For isotopic analysis, each core sample was cut to size and pulverised into a fine silty powder. Sections of core that were considered to accurately represent the bulk rock at that depth interval were pulverised in a ring mill into a fine homogeneous powder. Sub-samples were taken from the powder and sent to GNS for oxygen ($\delta^{18}O$) and hydrogen (D or ^{2}H) isotopic analysis.

A CO_2-laser in conjunction with BrF_5 was used to separate the oxygen from the sample, ultimately providing quantified values of $\delta^{18}O$. The $\delta^{18}O$ values were reported relative to Vienna Standard Mean Ocean Water (VSMOW) and normalised according to the NBS-28 international quartz standard (+ 9.6‰), with each of the 4 analysed NBS-28 standards not exceeding a range of +0.15‰. Before being placed into the vacuum line of the CO_2–laser, the standards and samples were heated to $150^{0}C$ for approximately 12 hours. The extraction line once loaded with samples was then vented for a period of 6 hours. To ensure oxygen values were accurately reflected from the sample's composition only, blank runs of BrF5 were used until <0.2 µm O_2 were detected. Finally, a Geo20-20 mass spectrometer was used to analyse and obtain the Oxygen data derived from CO_2 gas.

^{2}H (presented as δD) values were obtained from a GV Instruments IsoPrime mass spectrometer in conjunction with a HEKAtech high temperature elemental analyser. Prior to loading, all samples and standards were thermochemically decomposed inside silver containers at 1450^{o}C. The isotopic composition of the samples is presented relative to VSMOW. The international Standards NBS22 (δD -118‰), NBS30 (δD -66‰) and IAEA-CH-7 (δD -100 ‰) were used to normalise the data. Furthermore, the data was also normalised with respect to international water standards W62001, ISGS46, USGS47 and USGS48 with δD values of -41.1‰, -235.8‰, -150.2‰, and -2.0‰ respectively.

The remaining powdered samples were weighed out and spiked with $^{147}Sm/^{143}Nd$ spike H, then dissolved in a mixture of 28M HF and 15M HNO3 at a 2:1 ratio. The capped solution was left on a hot plate at 140^{o}C for 48 hours. The sample was evaporated and dissolved once more in HF and HNO_3. Once evaporated a second time, the samples were re–equilibrated and dissolved in 1ml of 2M HCL. The HCl solutions were loaded into cation-exchange columns with BioRad AG50W-X8 resin. Once rare earth elements (REEs) were separated from the bulk rock, the remaining solution was passed through Eichrom Ln Spec resin columns to separate the Sm from the Nd. The Nd was mixed with a Sm-Nd loading solution comprised of 1M HNO_3 and 1% H_3PO_4, and loaded onto rhenium filaments. Isotopic analysis was then conducted on an Isotopx phoenix x62 Thermal ionisation mass-spectrometer (TIMS) at the University of Adelaide. The standard BHVO-2 (USGS Basalt) was used, and produced a mean $^{143}Nd/^{144}Nd$ of 0.512974 which is consistent with the University's long term average of 0.512973.

The true JNdi-1 values were used to normalise the $^{143}Nd/^{144}Nd$ spike corrected data (Goldstein et al., 1984). The Nd standard JNdi-1 was used, and produced a mean 143Nd/144Nd of 0.5121057. The true value of 0.512108 is consistent with the average of the facility over a long time span dating back to January 2015 gives a value of 0.512107. The contamination levels of Nd and Sm were 298 pg and 170 pg respectively – falling well under the permitted maximum value of 1ng each. Such small values are considered statistically insignificant and do not adversely affect the results.

Laser-Ablation Inductively-Coupled Mass Spectrometry (LA–ICP–MS) was used on particularly garnet-rich sections of core that were cut to 10–20mm sized pieces, and cast into grain mounts and then polished. Spot analyses were conducted upon garnet-containing grain using an Agilent 7500x ICP-MS with attached New Wave UP-213 laser system. This also provided trace element maps of garnets generally ranging in size from 3 to 10 mm in diameter.

The polished garnet blocks were analysed under a Cameca SX–Five electron probe microanalyser (EPMA) at Adelaide Microscopy. The EPMA's beam current was 20nA with an operational voltage of 20kV.
Back-scattered electron (BSE) images were generated on a FEI Quanta 450 scanning electron microscope (SEM) with the ability to capture BSE images.

OBSERVATIONS AND RESULTS

Petrography

The primary lithology of interest in the SAR8 region is a skarn, divided into three sub groups: garnet skarns, pure skarn, and mineralised skarns. Through the interval of interest (950–1271m) the skarn is quite mineralised and very garnet rich. Garnet abundance and size appears not to follow a strict relationship, but occurs in bands and clusters intermittently dispersed throughout SAR8.

The approximately 300m thick interval of skarn in SAR8 is situated beneath the GRV and above the Donnington suite, and intermittently intruded by the HIS, though no sections of pure HIS exist within SAR8 (Mason et al., 1983). The garnets within the skarn range in size from 1mm to 20mm, often making up a majority of the rock in which it resides. Aside from aforementioned banded garnet intervals, massive and porphyroblastic garnet textures similar to those at Punt Hill (Nikolakopolous, 2013) are also observed throughout, with no apparent spatial relationship between abundance and mineralisation. The skarn itself is characterised by shades of green, red, and brown, and visibly altered, rarely preserving any sedimentary structures or features.

The weakly metamorphosed rock is incredibly altered, predominantly featuring scapolite-albite alteration, calc-silicate, haematitic, sericitic, propyllitic, potassic and chloritic alteration (Mason et al., 1983), the former indicating the original Wallaroo stratigraphy was partially comprised of evaporites (Reid et al., 2009). This style of alteration is similar to that seen at Olympic Dam and Punt Hill (Reid et al., 2011;

Schwartz, 2010). Furthermore, this alteration appears not to follow any trend with regards to composition or depth of the whole rock.

SKARN

Pure skarn refers to the composition of the metasomatised rock in which mineralisation and garnets reside. The skarn is particularly fine grained with an average grain size of approximately <1mm. The primary minerals that comprise the skarn are carbonates, talc, amphibole, fluorite, chlorite, potassium feldspar, and quartz. Accessory minerals such as titanite have also been observed intermittently dispersed throughout the skarn. Calcite, quartz and chlorite frequently appear to replace other minerals within the skarn and appear at times as small veins. When accumulated within the skarn, high concentrations of amphibole form radial patterns, and indicate crystallisation occurred after the formation of sulphides. Aside from K-feldspar, plagioclase is also present nearly exclusively as albite. Feldspars within SAR8 occur in small layers and are patchy, diminishing in frequency with depth, and becoming less frequent close to peak mineralisation. The skarn at various depths in SAR8 is heavily brecciated and cross cut by calc-sillicate veinlets.

GARNET SKARN

The mineralised interval of interest within SAR8 is highly abundant in garnets, and is referred to as a garnet skarn when the amount of garnet exceeds the amount of pyroxene. There is no strict relationship between the frequency, and size of garnets throughout SAR8 in relationship to depth or mineralisation intensity as mentioned previously, however the amount of garnet rapidly diminishes after peak mineralisation has been reached. The general composition of the skarn does not change greatly with

the abundance of garnet and despite being an overall heterogeneous rock, the skarn's general composition does not differ excessively. The abundance of garnet is variable, with high concentrations of garnet occurring in banded layers, defined as garnetite. Throughout the garnet skarn, inclusive of garnetite layers, the textures of garnets vary greatly, often overprinting, cutting and replacing other minerals. Garnets are also overprinted and cross cut by feldspars and various kinds of alteration, as well as sulphides, but are rarely intersected by quartz or carbonate veinlets. Replacement of garnets by calcite and feldspars that comprise the skarn is apparent in some areas. Garnets in Pernatty Lagoon are frequently overgrown and corroded by sulphides, potassium feldspar, talc and calcite. Inclusions of apatite, titanite and zircons can be found within garnets.

MINERALISED SKARN

The most prominent mineralisation found in the skarn in Pernatty Lagoon is chalcopyrite. Chalcopyrite and pyrite often occur together. Galena and sphalerite also occur in relatively high abundance throughout the core (Figure 3). Traces of silver and gold are present, though in small concentrations of ppm and ppb respectively (Appendix A). Haematitic alteration occurs throughout the core not conforming to a pattern or trend. The disseminated iron oxide often stains surrounding mineral phases and is not present in economic concentrations.

Sulphide mineralisation occurs as cm scale clusters, or finely disseminated throughout the skarn. Peak copper mineralisation occurs at approximately 1148m depth in which sulphides form large veins and aggregates up to 6mm across, amongst the already prevalent disseminated sulphides. At shallower depths the sulphides become much more

disseminated and the veins diminish in size and frequency. Galena and sphalerite occur largely together but tend not to be abundant in areas of very high copper concentration. Sulphides such as chalcopyrite, galena and sphalerite overprint garnet rims and are found within garnet grains as inclusions seen in Figures 3 and 14. It is important to note the mineralisation in Pernatty Lagoon is of sub-economic grade.

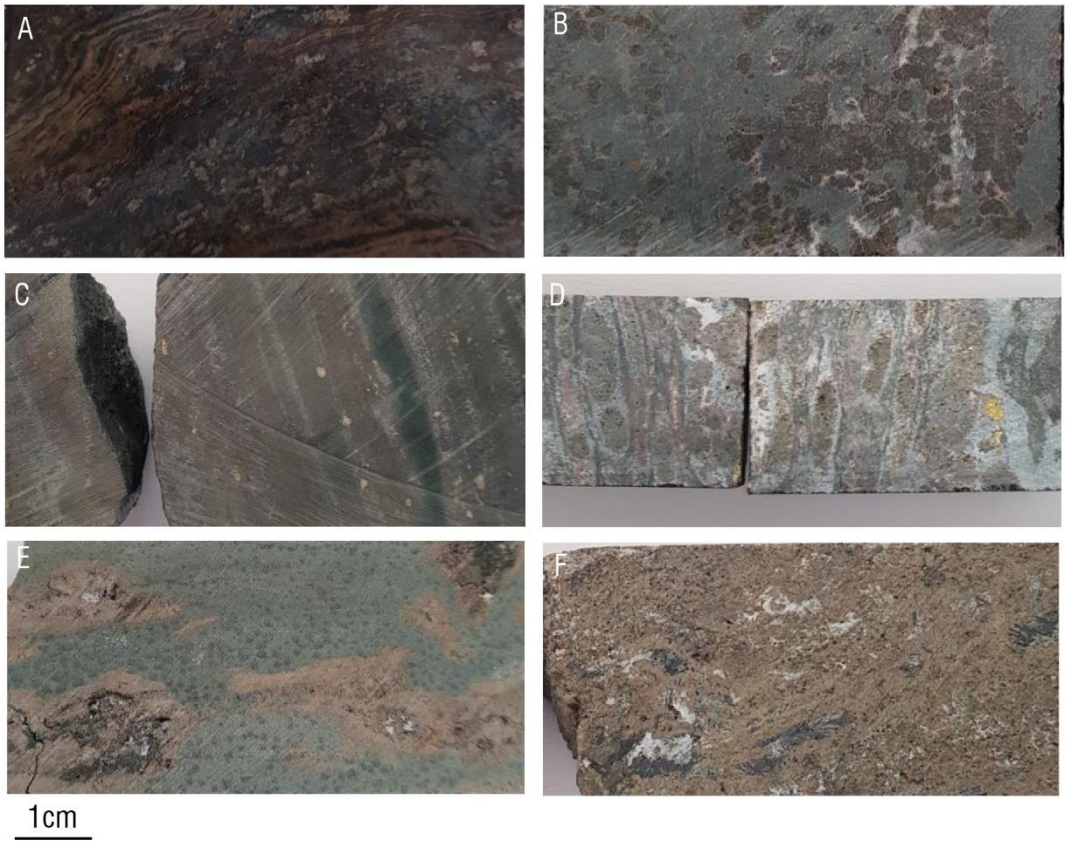

Figure 3: Images of core face-slices from SAR8 which were later used for isotopic and REE analysis. A) peak copper mineralisation, disseminated and crystallised sulphur including chalcopyrite, pyrite, sphalerite and trace galena. Garnets are present scattered throughout. Shows actinolite-hematite altered skarn. B) garnetite assemblage with silicate and calcite infill, and abundant pyroxene-chlorite alteration. Chloritic alteration of garnets is visible with occasional calcite veining. C) mineralised siltstone with rare chloritic-pyroxene veining and occasional large calcite crystals. D) pyroxene-chlorite-skarn altered calc-silicate rock with occasional chalcopyrite crystals present. Pale brown garnet overgrowth of yellow garnets. Chlorite-pyroxene alteration visible around garnets. E) heavy chlorite-pyroxene alteration of unmineralised skarn, overprinting garnets. Trace amounts of fluorite present as crystals. F) pyroxene-actinolite-calcite altered skarn with occasional garnet present.

RESULTS

STABLE ISOTOPES

Stable isotope data for δD and $\delta^{18}O$ was conducted on twenty samples taken at various depths within SAR8 from 974.7 to 1269.3 metres. The sample depths and their corresponding Cu, Pb and Zn values are given in Table 2. δD and $\delta^{18}O$ values were obtained from rock powder samples using processes described above in methods, and are presented in Table 2. The obtained $\delta^{18}O$ values were plotted against copper concentration in Figure 4. Initially at low copper concentrations the $\delta^{18}O$ varies greatly, mostly encompassing values between 8 and 14‰. After this initial clustering of data points at low Cu concentrations, Cu content begins to gradually increase as $\delta^{18}O$ decreases. Similarly for δD in Figure 5 low concentrations of Cu are dispersed erratically but tightly and follow no trend with δD. However, the δD becomes more positive as Cu concentration increases, before reaching a peak and then becoming more negative once more with increasingly higher concentrations of copper – leading to a more bell-shaped distribution, and following a similar trend to Cu and $\delta^{18}O$. There is no apparent correlation between $\delta^{18}O$ or δD and depth, Lead concentrations, or Zn concentrations.

When plotted against one another $\delta^{18}O$ and δD plot very closely together, but don't follow a distinct relationship. The outlier of the main trend in Figure 6 is sample 8088 and has the most isotopically light $\delta^{18}O$ and δD, as well as highest concentration of Cu.

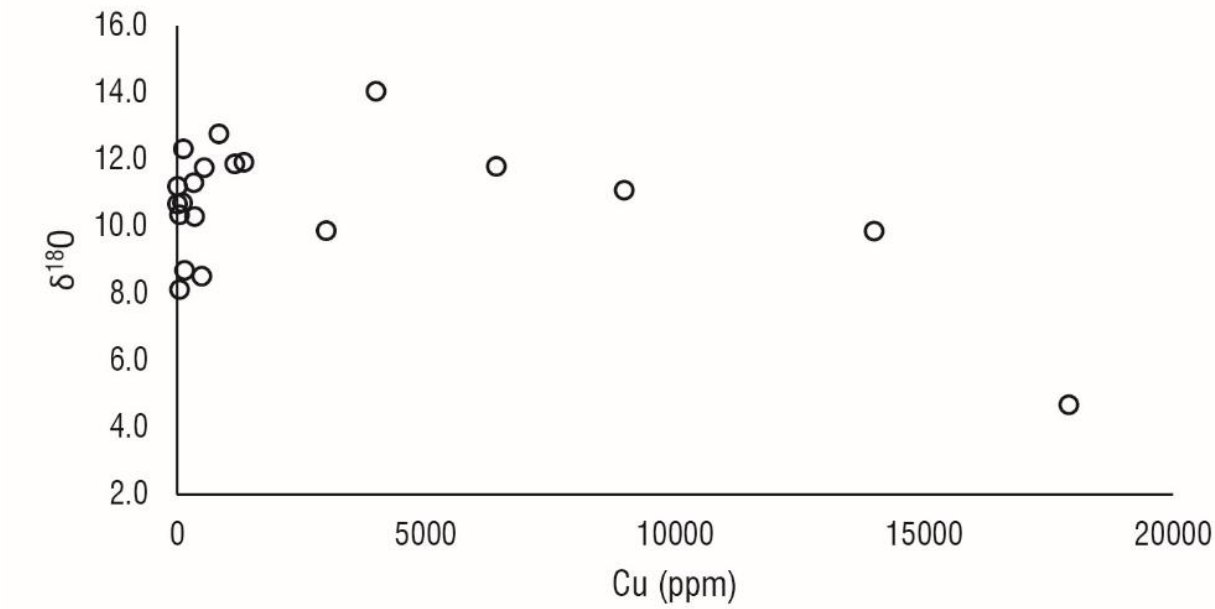

Figure 4: $\delta^{18}O$ (‰) compared to copper concentration in SAR8, showing initial grouping followed by a distinct trend in which copper increases with decreasing $\delta^{18}O$.

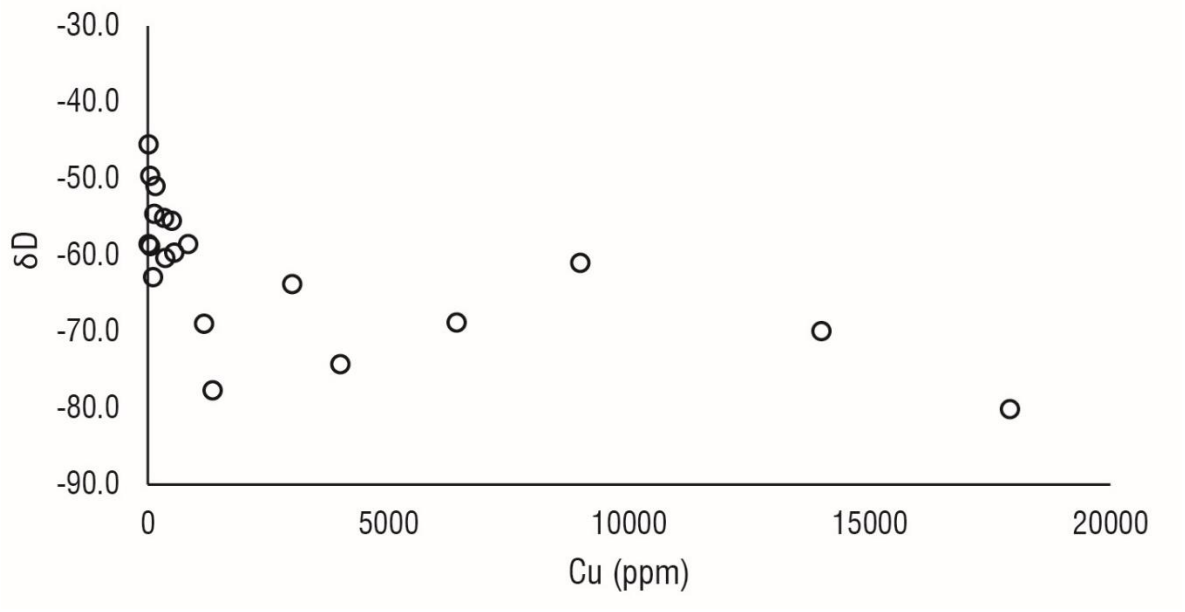

Figure 5: δD (‰) compared to copper concentration in SAR8, showing initial grouping followed by a distinct bell-shape trend in which increasing copper results in isotopically heavier, and then lighter values of δD.

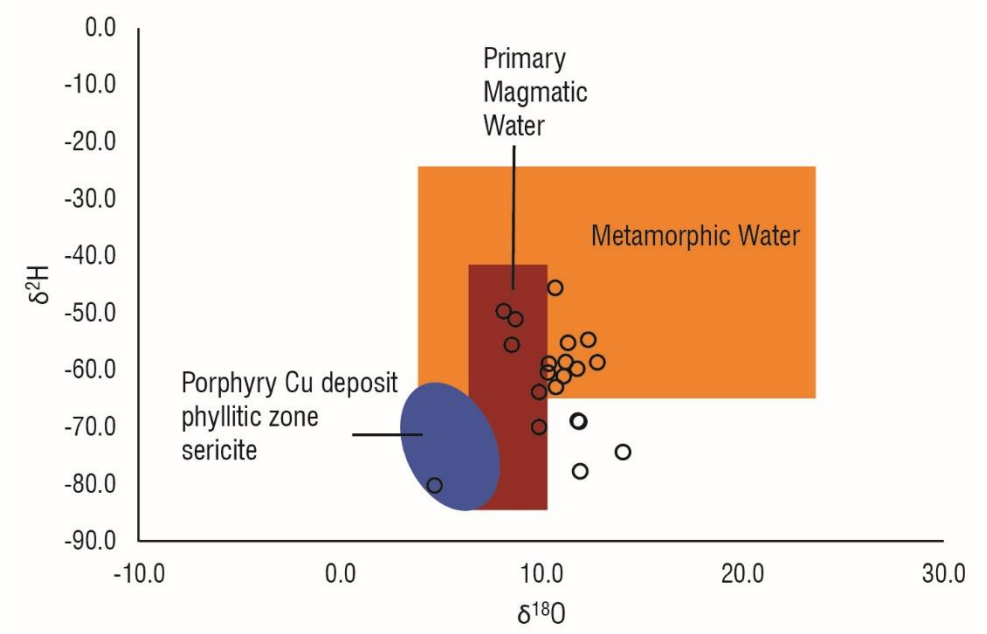

Figure 6: $\delta^{18}O$ compared to δD, showing central grouping. The point in the bottom middle separate from the central grouping represents sample 8088 (peak Cu mineralisation). Modified from (Sipahi et al., 2017).

Table 2: Stable isotope data for twenty samples in SAR8 showing corresponding depth values and concentrations of Cu, Pb and Zn.

Sample	Depth (m)	δD (‰)	$\delta^{18}O$ (‰)	Cu (ppm)	Pb (ppm)	Zn (ppm)
8063	974.7	-45.5	10.7	13.5	63	800
8075	1049.7	-68.9	11.9	1164	170	882
8076	1059	-58.5	12.8	840	850	3300
8077	1069.3	-55.1	11.3	340	1200	5354
8078	1079.3	-62.9	10.7	111	200	736
8079	1088.1	-54.6	12.3	130	51	120
8082	1109.6	-60.3	10.3	360	61	1000
8083	1118.8	-59.7	11.8	552	1100	3373
8084	1124.6	-63.8	9.9	3000	500	1800
8085	1129.9	-68.8	11.8	6417	80	247
8086	1135.4	-74.3	14.1	4000	240	600
8087	1138.4	-77.6	11.9	1347	406	807
8088	1148.5	-80.1	4.7	17913	84	278
8089	1149.7	-69.9	9.9	14000	95	280
8090	1153	-61.0	11.1	8985	117	300
8091	1159.4	-58.8	10.4	52	137	299
8093	1176.3	-55.5	8.5	500	730	1600
8097	1210.1	-51.0	8.7	157	500	1160
8099	1222.5	-49.6	8.1	50	1200	800
9000	1269.3	-58.5	11.2	12	53	546

RADIOGENIC ISOTOPES

Sm–Nd isotope data for mineralised bulk rock in Pernatty Lagoon was conducted on ten samples from SAR8 in Pernatty Lagoon alongside one blank sample and one USGS standard. The ten samples were representative of skarn mineralisation from the interval 974.7 to 1269.3 5m at varying levels of copper concentration. The corresponding drill core depths, sample numbers and amount of Nd are listed in Table 3. The εNd was calculated using the equation below and the model and values from Goldstein et al (1984).

$$\varepsilon Nd = \left[\frac{(^{143}Nd/^{144}Nd)_{SAMPLE}}{(^{143}Nd/^{144}Nd)_{CHUR}}\right] \times 10000$$

Equation 1: Calculating εNd from sample values obtained from Pernatty Lagoon. Using model values from Goldstein et al (1984).

$^{143}Nd/^{144}Nd$, $^{150}Nd/^{144}Nd$, $^{147}Sm/^{149}Sm$, and $^{152}Sm/^{149}Sm$ values were obtained from TIMS and normalised to produce εNd values. These were plotted and compared to copper mineralisation, and showed a lack of a strong relationship between the two. There was no discernible or significant change with respect to Cu concentration as a result of εNd. The distribution of the two is relatively flat, though slightly bowl-shaped with an average εNd of -6.68.

Similarly, there is no correlation between mineralisation of other metal sulphides such as galena or sphalerite and εNd. The radiogenic isotope results for Nd and Sm are within the range of two stand errors. The εNd(t) values were calculated at age 1577$\pm$7 Ma as this is the age at which it is believed the skarn of Pernatty Lagoon formed (Fabris et al., 2016; Reid et al., 2011; Skirrow et al., 2007).

Comparing copper concentration against depth concurrently with εNd shows an overall bowl-like trend similar to the one seen above in Figure 7. Initially, at low Cu concentrations, an increase in Cu concentration is echoed by a positive increase in εNd, and likewise for a decrease in Cu concentration. Upon reaching higher levels of Cu within the rock at approximately 1130m depth the relationship between Cu and εNd appears to reverse – with Cu increasing as εNd becomes more negative. This anomalous and alternating trend is mirrored throughout the interval of peak mineralisation until approximately 1160m where the Cu content diminishes down to approximately 52 ppm and the trend reverts to the original coupled trend seen prior to peak mineralisation. The least most altered samples are represented by the first and last samples within Figure 7.

Contrastingly, the pattern between the mineralisation of Zn and Pb behaves in an opposite manner to that of Cu, in which the εNd trend follows the same pattern as the Zn and Pb concentration trends do during peak mineralisation (Figure 10). The relationship between εNd and Pb and Zn prior to and after peak mineralisation does not seem to follow a strong trend. It is important to note that in the interval of peak mineralisation for Cu, Pb and Zn, the more negative values for εNd correspond to higher concentrations of Cu, more positive values for εNd correspond to higher concentrations of Zn and Pb. To simplify, positive changes in εNd correlate to less Cu but more Pb and Zn, and vice versa.

The $^{147}Sm/^{143}Nd$ and $^{143}Nd/^{144}Nd$ values were plotted against each other, showing a relatively linear relationship between the two ($R^2 = 0.8616$) in Figure 11. A majority of the data points are clustered to the lower left-hand corner of the graph, corresponding to

relatively low $^{147}Sm/^{144}Nd$ and $^{143}Nd/^{144}Nd$ values. Two values occur as polar opposites in the upper right corner of Figure 11 and represent samples 91 and 88 respectively from left to right. These anomalously high values were over spiked during the sample preparation process due to their very low Nd content. Despite this they were corrected for the purposes of calculating εNd. The point highlighted above in Figures 11 and 12 represents the USGS standard BHVO-2. The data from Figure 11 has been overlain with values from Goldstein et al., (1984) in Figure 12 to show the maturity of radiogenic isotopes in Pernatty Lagoon skarn.

Table 3: Radiogenic isotope data from SAR8 bulk rock samples. εNd calculated for the inferred age of skarn formation 1577 Ma (Reid et al., 2011).

Sample	Sm ppm	Nd ppm	$^{147}Sm/^{144}Nd$	$^{143}Nd/^{144}Nd$	2SE E-06	$eNd_{(1577\ Ma)}$
8063	6.44	28.51	0.136544	0.51163	1.80E-06	-7.55
8075	3.39	15.60	0.131252	0.511658	1.45E-06	-5.92
8083	4.51	36.60	0.074556	0.511024	2.21E-06	-6.83
8085	3.96	19.56	0.122328	0.511492	2.50E-06	-7.37
8087	2.84	18.09	0.095056	0.511293	1.78E-06	-5.72
8088	5.61	10.49	0.323231	0.513577	5.39E-06	-7.32
8090	3.34	14.99	0.134635	0.511656	3.98E-06	-6.64
8091	8.23	19.29	0.257983	0.512908	1.92E-06	-7.17
8099	1.68	10.45	0.097383	0.511314	3.44E-06	-5.79
9000	5.25	31.62	0.100392	0.511308	1.66E-06	-6.52

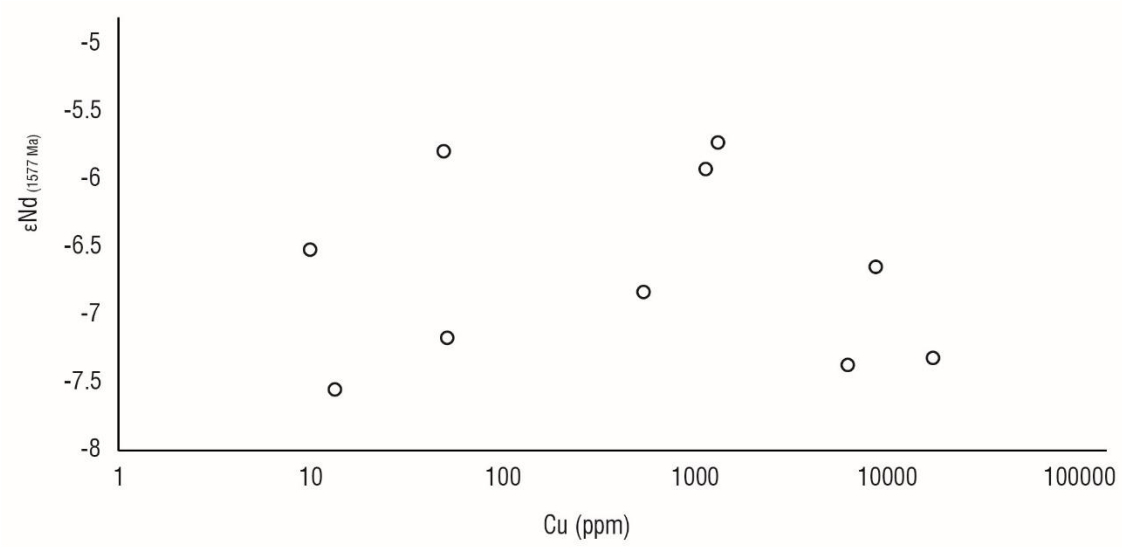

Figure 7: The relationship between copper concentration and isotopic signature of mineralised bulk rock in SAR8 showing no strong correlation and a somewhat bowl-shaped distribution.

Table 4: Assorted εNd values from various materials within the Gawler Craton. Data obtained from (Cave, 2010; Howard et al., 2009; Johnson, 1993; Nebel et al., 2007; Reid et al., 2011; Skirrow et al., 2007).

εNd	Sample Material	Location	Source
-2.5	Hematite-rich rock	Olympic Dam	Johnson, 1993
-4.9	Magnetite Breccia	Olympic Dam	Johnson, 1993
-5	Fresh Granite	Olympic Dam	Johnson, 1993
-0.3	Bornite-Chalcocite Ore	Olympic Dam	Johnson, 1993
-2.7	Hematite-Quartz-Breccia	Olympic Dam	Johnson, 1993
-3	GRV	Stuart Shelf	Johnson, 1993
5	GRV	Stuart Shelf	Johnson, 1993
-3.1	Pandurra Sandstone	Stuart Shelf	Johnson, 1993
-5	HIS Granitoid	Stuart Shelf	Johnson, 1993
-9	HIS Granitoid >70% SiO2	Olympic Dam	Skirrow et al., 2007
-4.4	HIS Granitoid	Olympic Dam	Skirrow et al., 2007
-2.3	HIS Mafic Dyke	Olympic Dam	Skirrow et al., 2007
-6.4	GRV	Olympic Dam	Skirrow et al., 2007
-5.1	Lower Wallaroo	Stuart Shelf	Skirrow et al., 2007
-6.6	Unaltered Wallaroo	Stuart Shelf	Skirrow et al., 2007
-19.78	Hematite-Calc silicate	Punt Hill	Reid et al., 2011
-20.31	Hematite-Calc silicate	Punt Hill	Reid et al., 2011
-5.7	Bulk Rock	Punt Hill	Reid et al., 2011
-38.41	Diopside	Punt Hill	Reid et al., 2011
67.1	Garnet	Punt Hill	Reid et al., 2011
-4	Paragneiss	Corny Point	Howard, 2009
-5.98	Myola Volcanics	Moola	Cave, 2010
-2.63	Myola Volcanics	Moola	Cave, 2010

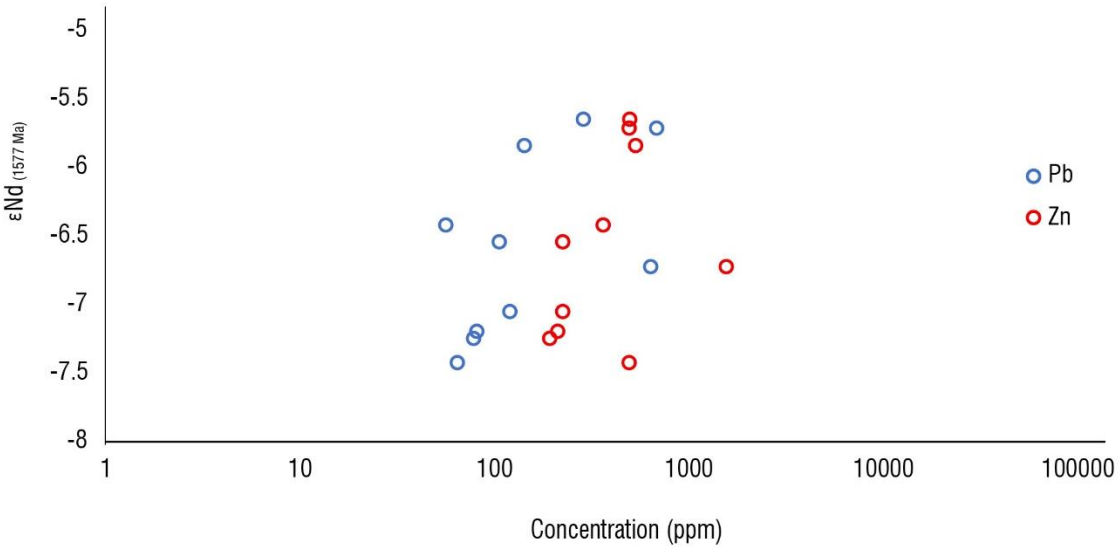

Figure 8: The relationship between zinc and lead concentration and isotopic signature of mineralised bulk-rock in SAR8 showing a weakly linear correlation.

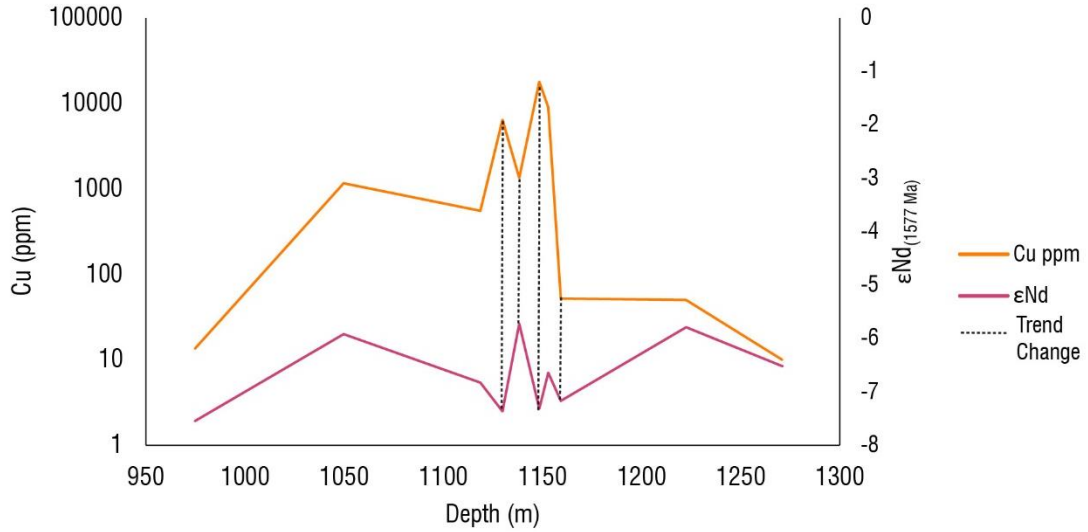

Figure 9: Behaviour of general copper concentration and εNd coupling and decoupling trends as a function of depth downhole in SAR8.

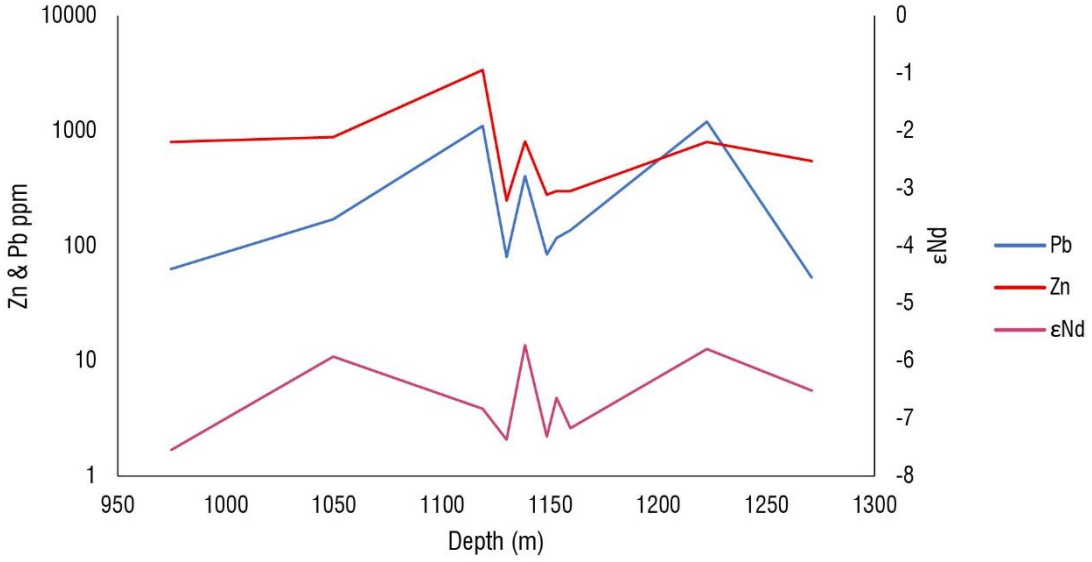

Figure 10: Coupling and decoupling of Zn, Pb and εNd as a function of depth downhole in SAR8.

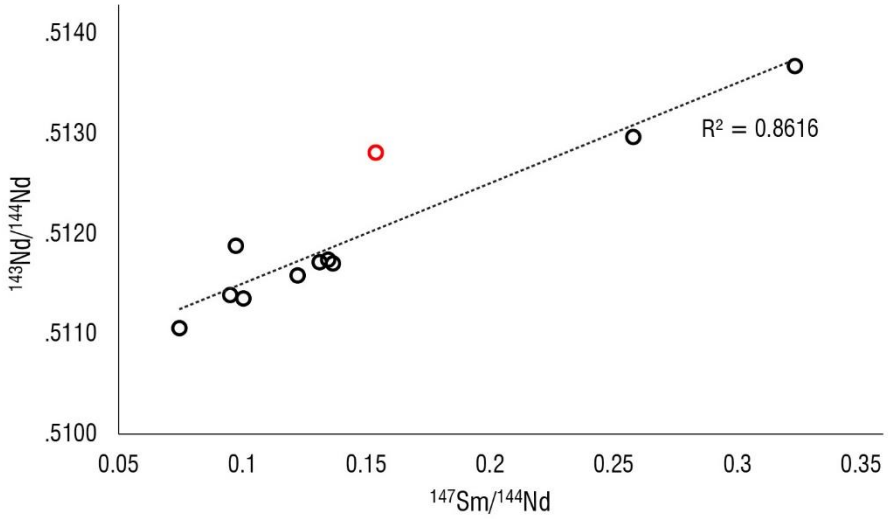

Figure 11: Radiogenic isotope fractionation trends in bulk rock samples in SAR8. The data point highlighted in red represents the value obtained from the USGS standard BHVO-2

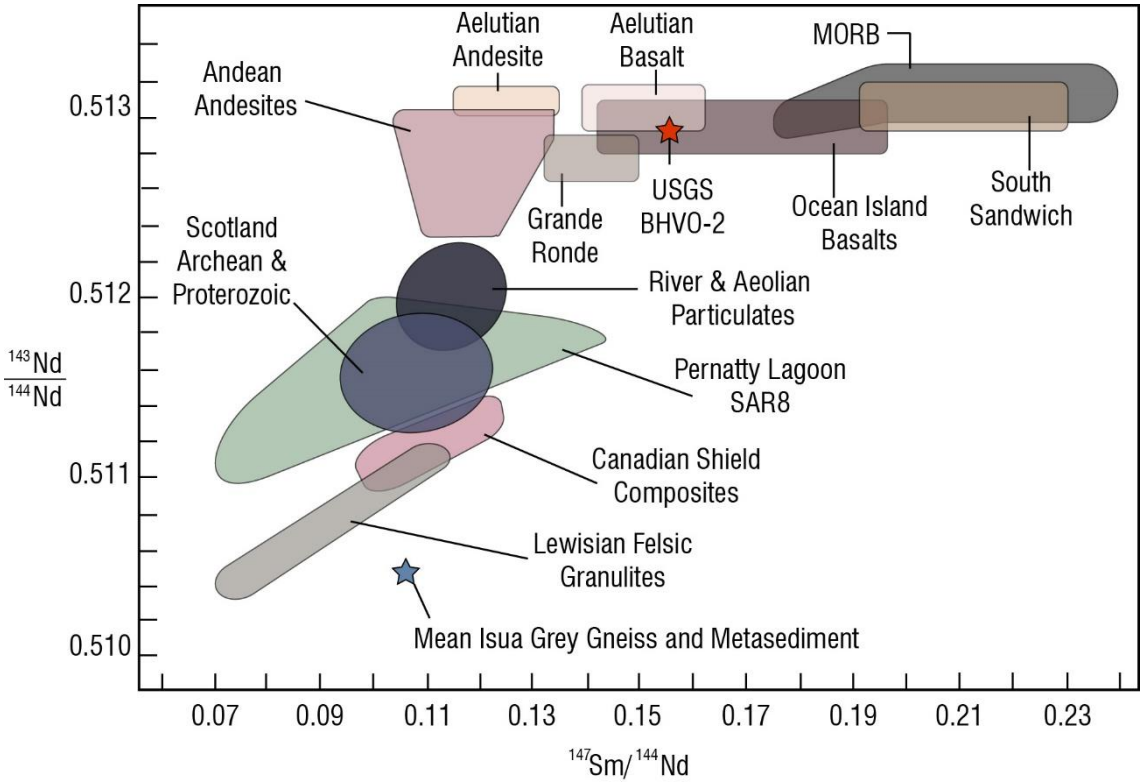

Figure 12: Sm/Nd isotope data compared to global standard values. The left-hand side indicates more fractionated values. The USGS standard used in this study (BHVO-2is denoted by the red star. Its appropriate location on the graph as a basalt indicates the validity of the radiogenic isotope data. The clustering and locations of the data (green) is echoed by εNd values. Two major outliers that exceed the range of this graph have been excluded. Modified from (Goldstein et al., 1984)

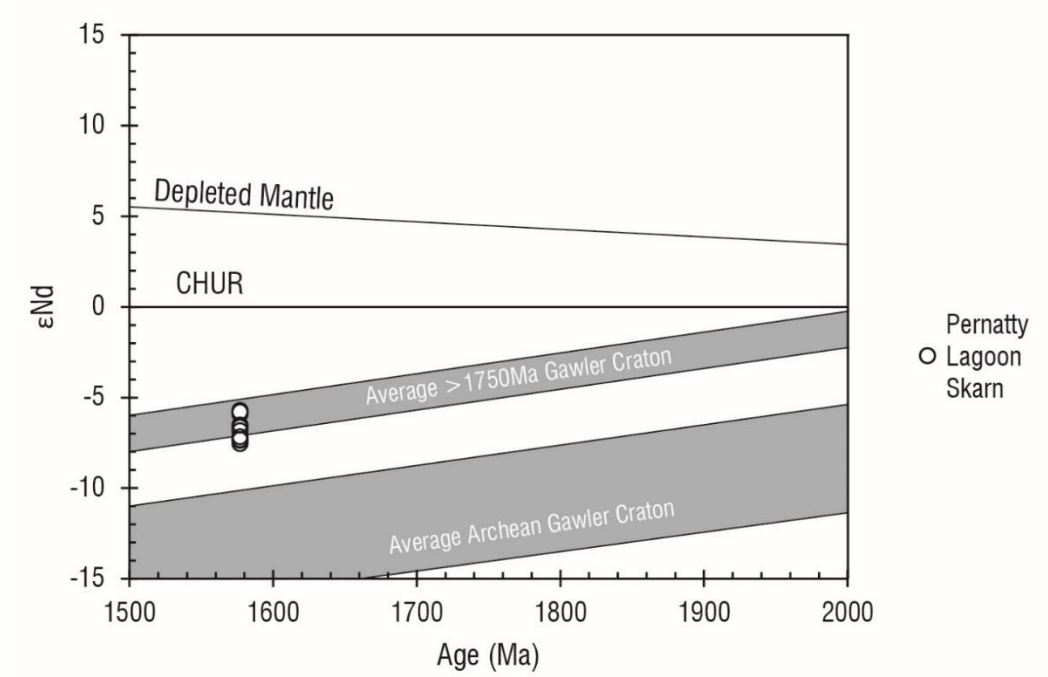

Figure 13: εNd evolution diagram of 1577Ma Pernatty Lagoon Skarns in SAR8 compared to average εNd in the Gawler Craton.

TRACE ELEMENTS AND REE

The REE abundance in SAR8 is normalised to McDonough and Sun (1995) and is stated with respect to the core or rim of the garnet. Relative to LREEs, HREEs are comparatively depleted in the system, with the abundance of LREEs when normalised to CHUR significantly exceeds HREEs in most cases. The abundance of HREEs is inconsistent between rims and cores, with the latter being typically enriched in LREEs. Of the lanthanide series, Sm is relatively depleted, and is likely due to decay into Nd. La is also significantly and consistently depleted relative to other lanthanide elements across all samples as seen in Figures 15, 16 and 17. Relative to other LREEs, Ce is also frequently depleted however not to the same extent. Positive Eu anomalies exist in both the rims and cores and garnets with no particular observable relationship between the two, however these anomalies always coincide with a negative Sm anomaly, and vice versa in both rims and cores. Furthermore, negative Eu and thus positive Sm anomalies coincide consistently with observably more depleted La and Ce, with a more pronounced trend visible in rims rather than garnet cores. HREEs are distributed more flatly with respect to LREEs in both rims and cores, with little to no anomalous spikes. The respective enrichment or depletion of Sm, Eu, La and Ce is not correlated to the distribution and pattern of HREEs. The cores of garnets are significantly more enriched in LREEs and are considerably more depleted in HREEs with respect to garnet rims. By comparison, the rims have a flatter distribution of REEs. In both rims and cores, the distribution of HREEs is partitioned and separated by an order of magnitude, generally corresponding to a greater amount of LREEs.

Electron microprobe data determined that the garnets within SAR8 are dominantly andradites, with compositional values ranging from 56.15% to 98.68% (Table 5); (full

EMPA data can be found in Appendix A). The composition of the garnet core is largely definitive of garnet composition, as most garnets that are <85% andradite and more grossular respectively have more Al enriched cores. This is indicative of iron enrichment in prograde growth of garnet, and retrograde aluminium rich growth of garnets.

According to Figure 17, garnets in the region of peak mineralisation in which Cu content exceeds 1000ppm have a flatter and 'tight' distribution. The distribution of both LREEs and HREEs are relatively more confined in mineralised garnets. There is no relationship between rims and cores in terms of positive Eu anomalies, as both rims and cores of garnets show this in mineralised and non–mineralised regions of SAR8. The average trends of REE in garnets within mineralised and non–mineralised regions of SAR8 can be seen in Figure 17 below.

Table 5: Type of garnet in Pernatty Lagoon determined from electron microprobe analysis.

Part of garnet	Sample number	% Garnet member		
		Andradite	Grossular	Spessartine
Rim	89	98.68451	0	1.3
Core	77	98.54613	0.101977	1.4
Core	78	98.48755	0.539785	1.0
Core	85	97.37889	1.642169	1.0
Core	91	96.23304	2.658165	1.1
Rim	85	93.66965	5.372557	1.0
Core	65	92.45318	6.411166	1.1
Core	87	92.07115	6.450951	1.5
Core	99	85.05586	13.60789	1.3
Rim	65	72.00423	26.38174	1.5
Rim	87	69.02181	29.29667	1.7
Rim	93	68.97082	29.4077	1.6
Rim	84	67.90981	30.06489	2.0
Core	84	67.85394	30.51076	1.6
Core	90	67.18966	31.24726	1.6
Rim	90	64.1869	34.2145	1.6
Core	89	61.83848	36.41671	1.7
Core	93	61.31798	36.80784	1.9
Rim	78	60.2444	37.99517	1.8
Rim	91	58.72782	39.48227	1.8
Rim	77	58.68204	39.5144	1.8
Rim	86	56.14554	41.81042	1.7

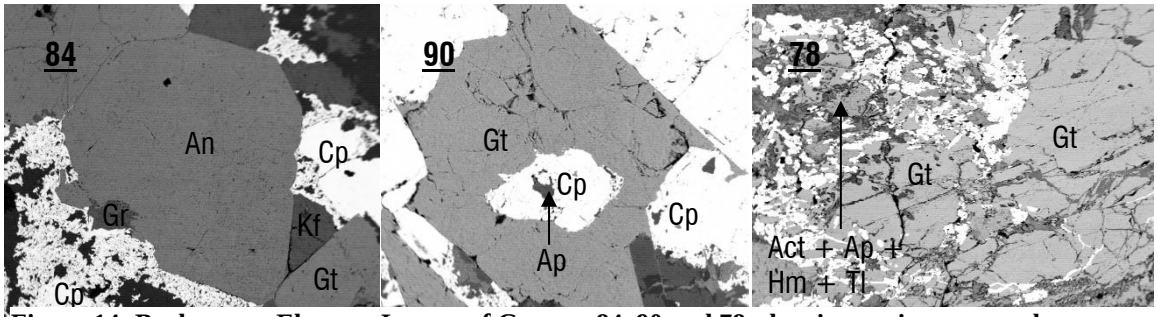

Figure 14: Backscatter Electron Images of Garnets 84, 90 and 78, showing various textural relationships between garnets and other minerals in SAR8 skarn. Garnet 84 shows zonation between Andradite and Grossular. Garnet 90 shows an apatite and sulphide inclusion as well as Sulphide overgrowth of rims. Garnet 78 shows extreme brecciation and fluid infill of various elements. Where Gr = Grossular, An = Andradite, Kf = K-feldspar, Gt = Garnet, Cp = Chalcopyrite, Ap = Apatite, Act = Actinolite, Hm = Hematite, Tl = Talc.

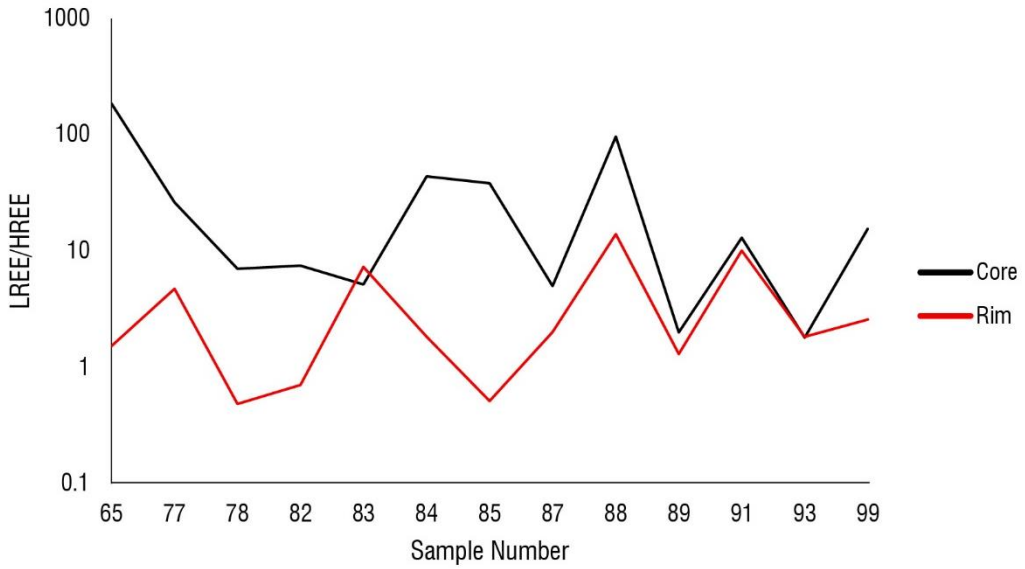

Figure 15: Relative LREE enrichment in garnets across samples in SAR8.

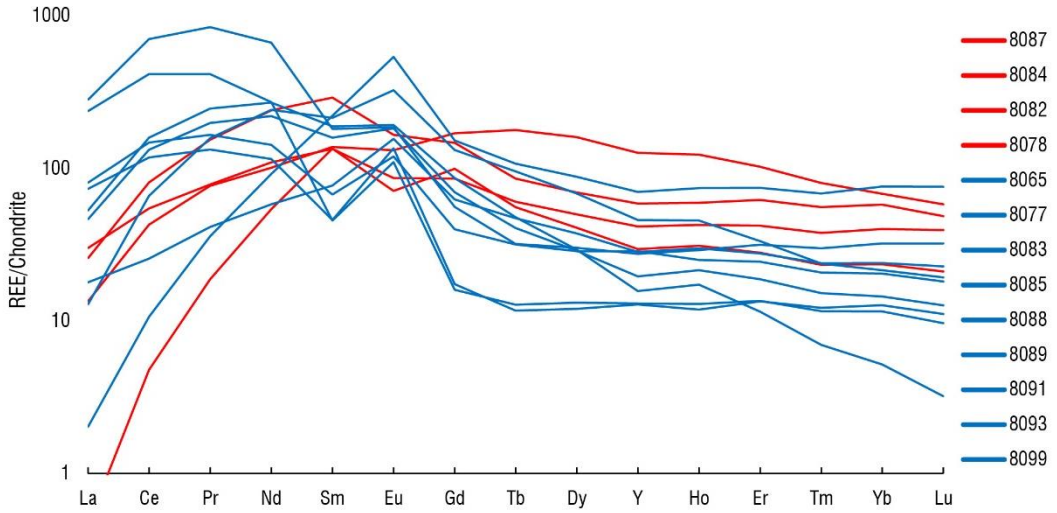

Figure 16: Spidergram of bulk garnets in SAR8 showing relative enrichment of REEs with negative Eu anomalies highlighted in red.

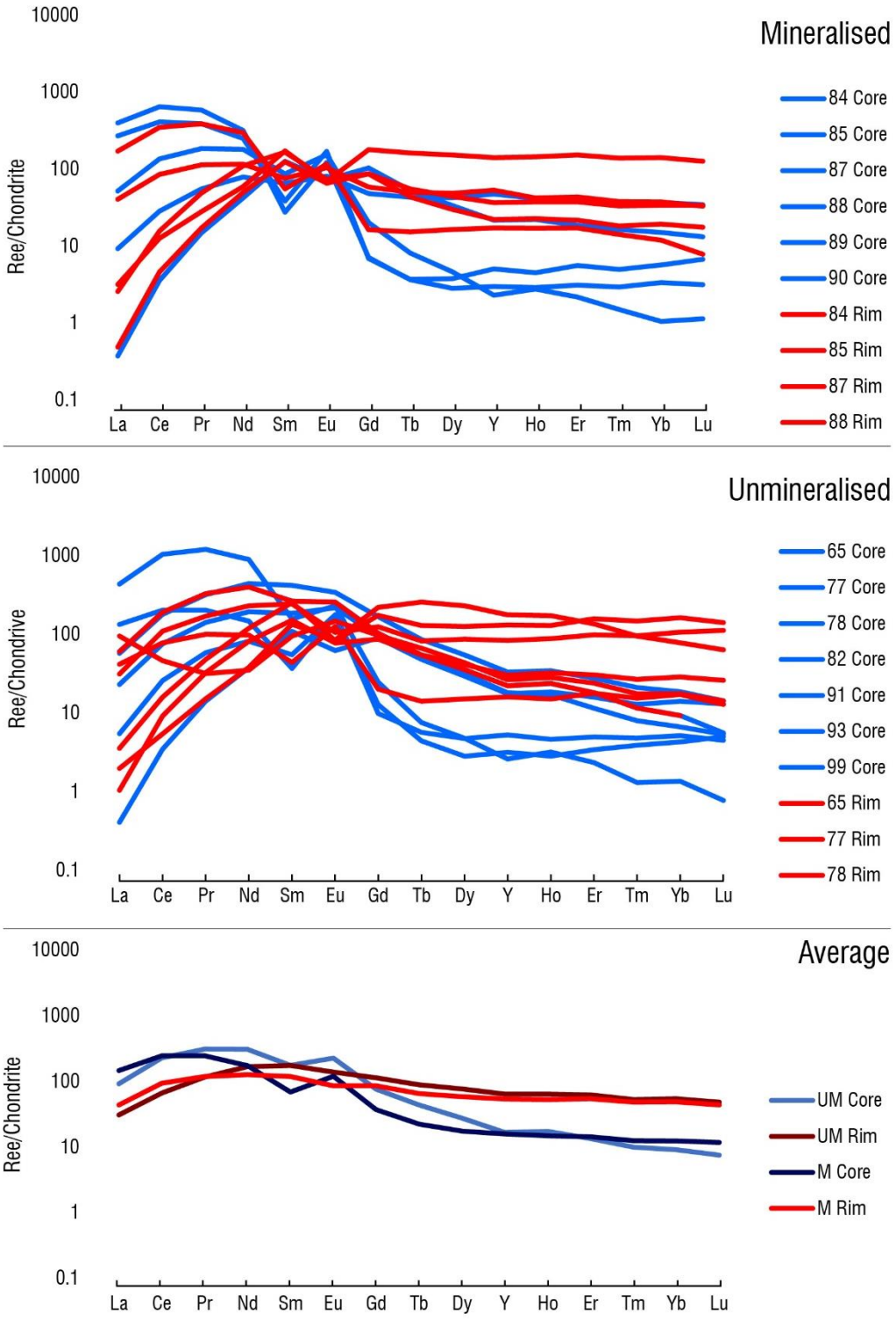

Figure 17: Spidergrams of garnets in mineralised and unmineralised horizons within SAR8 showing the differences between core and rim REE enrichment.

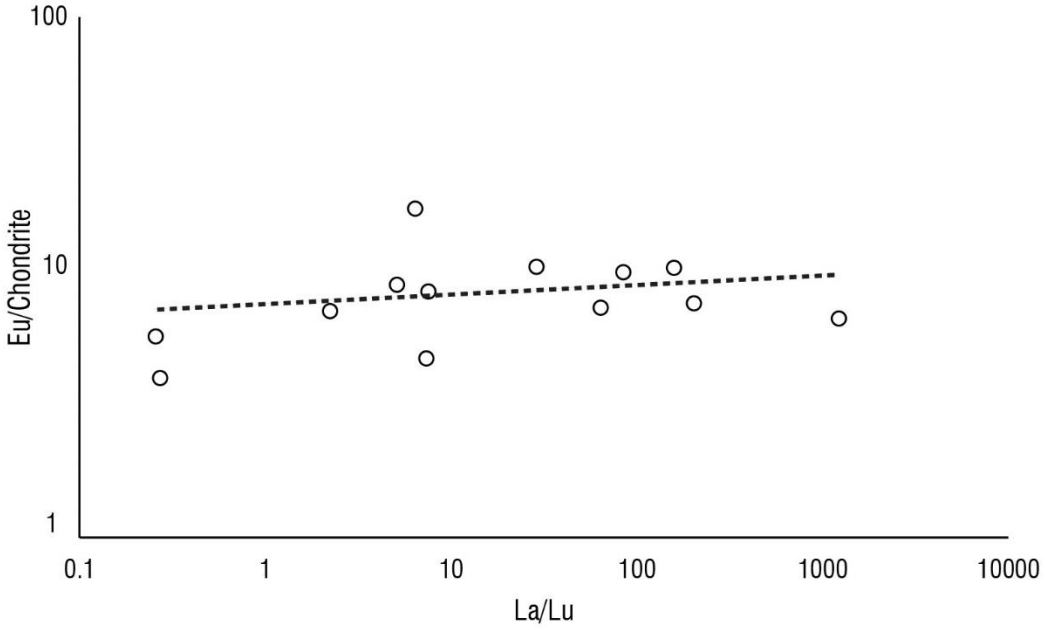

Figure 18: La/Lu compared to Eu content in garnets within SAR8.

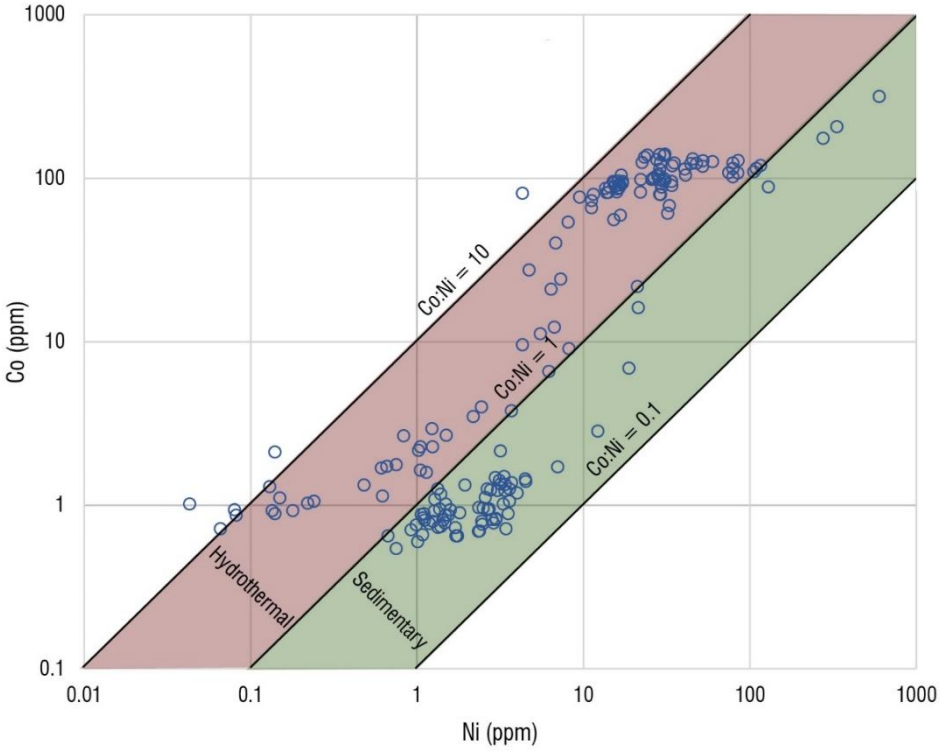

Figur **2008;**
Skirr

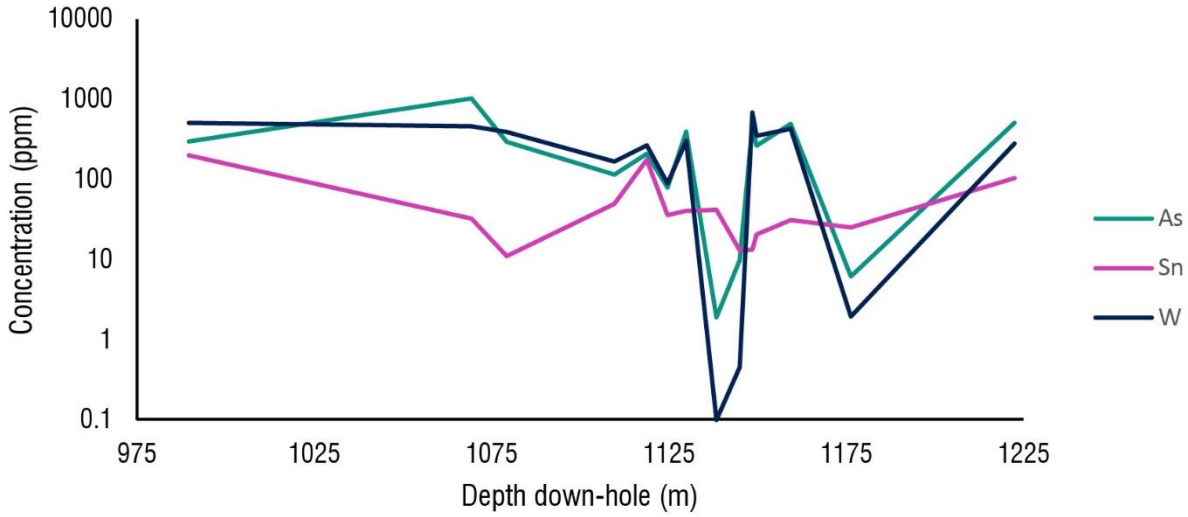

Figure 20: Abundance of select trace elements in SAR8 at depth downhole.

DISCUSSION

Stable Isotopes

Stable isotopes such as $\delta^{18}O$ and deuterium (δD) can be used to determine the nature of the fluid source of an orebody. As oxygen and hydrogen bearing minerals form, isotopic variation occurs due to fractionation through a variety of geological processes such as melting or degassing. When fluids enter a rock system, the characteristics of the fluid such as major element geochemistry and isotopic composition are reflected in the newly altered host-rock system. This can be seen in the Pernatty Lagoon skarn – alteration resulting from interaction between fluid and the Wallaroo Group metasediments. Typically, metamorphic and sedimentary rocks, metamorphic fluids, and metamorphic waters are enriched in heavier oxygen isotopes, whereas magmatic fluids, waters, rocks, volcanic rocks and meteoric waters are less enriched (Sipahi et al., 2017). Discerning between fluid sources can often prove to be a challenge, as the range of values that certain fluids and materials can take often overlaps with others. δD values for fluids and

rocks often span a much wider range of values than $\delta^{18}O$ comparatively, but can be used in conjunction with the latter to constrain and identify the nature of ore forming fluids (Wilkinson et al., 1995).

As can be seen in Figure 4, there are two distinct patterns between Cu and $\delta^{18}O$. The initial grouping of data at low copper concentrations is likely due to fluid interaction with metasediments, resulting in higher $\delta^{18}O$ values. The strong trend between $\delta^{18}O$ and Cu>5000ppm in Figure 4 is likely due to magmatic waters or fluids entering the system, and reacting progressively less with metasediments (Bastrakov et al., 2007). The $\delta^{18}O$ signatures approach magmatic compositional tendencies as concentration of Cu increases. The overall trend of δD and Cu is quite similar to $\delta^{18}O$ where increasing Cu concentrations correlate to isotopically lighter δD. The coupling of progressively lighter $\delta^{18}O$ and Cu was most likely the result of hydrothermal fluids forming as a result of magmatic degassing or fluid-basin interaction (Wilkinson et al., 1995). The grouped and weakly mineralised sections of SAR8 as seen in Figure 4 are likely to have such isotopically heavy values of $\delta^{18}O$ and δD from a mixture of metamorphic and magmatic fluids interacting with the shallower levels of rock in Pernatty Lagoon, post-dating peak mineralisation. It is possible but not proven that lithological traps were responsible for this almost bimodal distribution seen in Figures 4 and 5.

$\delta^{18}O$ and δD were plotted against one another in Figure 6. A vast majority of the data clusters in the centre, and resides in the *metamorphic water* range. The isotopic signatures for $\delta^{18}O$ at Pernatty Lagoon are very similar to other deposits in the Olympic Dam district, however the δD values vary greatly (Bastrakov et al., 2007). The more

mineralised regions of Pernatty Lagoon that correspond to more isotopically light values of $\delta^{18}O$ and δD plot in the range of *primary magmatic water*. The most mineralised sample (8088) did not plot in either the metamorphic or primary magmatic water range, but had a similar isotopic signature to sericites in the phyllitic zone of many porphyry Cu deposits (Sipahi et al., 2017). The region has a very complex tectonic history in which the rocks have been exposed to and altered by a variety of fluids. As sericitic alteration is prevalent throughout the rock, it is likely to be responsible for sample 8088 behaving the way it did.

Aside from regional metamorphic fluid input which seems into Pernatty Lagoon, it is possible that localised $\delta^{18}O$ enriched fluids from the HIS or GRV reacted with pre-existing metasediments of the Wallaroo Group, resulting in such high $\delta^{18}O$ signatures (Bastrakov et al., 2007; Hitzman et al., 1992). The vast difference between δD values in Pernatty Lagoon and the general Olympic Dam region are likely due to isotopic exchange between felsic igneous rocks and fluids, as the former typically increases δD values (Bastrakov et al., 2007; Hitzman et al., 1992).

Radiogenic Isotopes

Radiogenic isotope analysis of Sm/Nd isotopes can be used to analyse the isotopic interaction between previous fluid and rock interactions(Gleason et al., 2000). Sm/Nd analysis determines geochemical fingerprinting by determining the initial $^{143}Nd/^{144}Nd$ ratios from the decay of $^{147}Sm/^{143}Nd$ and provides information on the genesis of the rock. For isotopic comparison, individual minerals can be examined as well as whole

rocks – each of which has distinctly different isotopic compositions based upon their age, geochemistry and formation mechanism.

Typically, rocks derived from mantle materials tend to have a more primitive isotopic composition while those obtained from more crustally derived sources exemplify a more evolved composition equating to less Nd content (Goldstein et al., 1984; Howard et al., 2009; Skirrow et al., 2007). As can be seen in Figure 7. there was no correlation between Cu content and εNd indicating that it is likely that Cu and Nd were not transported in the same event, or that more than one fluid event occurred resulting in the mobilisation of some Nd (Cave, 2010; Johnson and McCulloch, 1995). The decoupling of Nd and Cu at Pernatty Lagoon means that whilst being from a crustal fluid source with minor mantle input, the Nd and Cu were not derived from the same fluid.

The εNd values at Pernatty Lagoon vary from -5.72 to -7.55 with an average of -6.68, indicating that the origin of mineralisation is of crustal nature with very minor mantle input (Johnson, 1993).

Similarly to this study, many others such as Skirrow et al., (2007) and Johnson & McChulloch, (1995) have compared the isotopic composition of predominantly IOCG deposits and prospects in the Gawler Craton to determine the fluid source of mineralisation. A range of εNd values for various rocks and minerals within the Gawler Craton was obtained and can be seen in Table 4 and Figure 13.

By comparison, the isotopic signatures of Olympic Dam give an εNd range of -4.9 to -0.3 with an average of -2.7 have a much more primitive and hence mantle-derived mineralisation source. Similarly, the Myola Volcanics of the Moola prospect 120km south of Olympic Dam have εNd values ranging from -5.98 to -2.63 with an average of

-4.05 (Cave, 2010). These values indicate that the mineralisation source fluid was more crustal derived with a slight primitive mantle input. Furthermore, a strong correlation between Cu and εNd can be seen both at Olympic Dam and Moola, where a linear relationship between Cu concentration and increasing εNd (more positive) values occurs (Cave, 2010; Johnson, 1993; Skirrow and Davidson, 2007). As this is not observed in the isotopically different Pernatty Lagoon region, it is possible that a correlation between Cu and Nd only occurs with more primitive and less evolved fluid sources, and that Pernatty Lagoon mineralisation is not related to the Olympic Dam IOCG deposit.

Work by Skirrow et al., (2007), Johnson & McChulloch, (1995) and Reid et al., (2011) reached conclusions similar to the one proposed below indicating the HIS or GRV generated mineralising fluids. As mentioned above, the isotopic signature of mineralised skarn at Pernatty Lagoon is approximately -6.68. This signature indicates that a more crustal source such as HIS, GRV or even Wallaroo Metasediments are responsible for mineralisation. The proposed fluid sources are more likely contenders than the fluid source observed at Moola or Olympic Dam not only for their more favourable radiogenic isotope geochemistry, but for their proximity as well.

Another possible mineralising fluid source at Pernatty Lagoon is thought to be responsible for the formation of skarn at the adjacent Punt Hill Prospect. Table 4 and Figure 13 show the εNd of the Wallaroo Group, GRV, and HIS. Their similarities with the average isotopic composition of Pernatty Lagoon are strongly indicative that they comprise one of potentially many components responsible for the mineralisation seen in Pernatty Lagoon. Temporal overlap and similar εNd between HIS and GRV indicates

that perhaps the formation of the GRV provided fluids for mineralisation. As the GRV overlies the Wallaroo group, percolated surficial or shallower fluids from the GRV could have entered through brecciated pathways to react with the Wallaroo Group.

In contrast, the HIS spans a much more concise and similar εNd range to Pernatty Lagoon, and contact as well as intrudes the Wallaroo Group in many instances. As Nd and Cu are decoupled and likely not from the same fluid source, it is likely that one of the two were derived from the HIS. The bulk Wallaroo Group sediments in Table 4 are also very similar to the Pernatty Lagoon crustal isotopic signature, and their interaction with the mineralising fluid(s) contribute to the overall evolved εNd in the mineralised horizon of Pernatty Lagoon. This interpretation is similar to that provided by Reid et al., (2011) and Nikolakopoulos (2013) in which the interaction between highly fertile Wallaroo group sediments and the HIS are thought to have been responsible for the mineralisation at Punt Hill. The bulk rock aside from petrographic similarities, the Isotopic composition of the two sites is relatively similar with an overall bulk rock εNd of -5.70.

The Punt Hill mineralisation and by extension the mineralisation at Pernatty Lagoon are thought to have occurred at the same time at approximately 1580 Ma (Nikolakopolous, 2013). Their very similar alteration styles and petrology as well as apparent syngenetic formation confirms that the two prospects have the same style of alteration as the event that resulted in the formation of many IOCG deposits in the Gawler Craton (Reid and Fabris, 2015; Skirrow et al., 2007) but due to isotopic differences likely had a different, more mantle-derived mineralisation source.

Contrary to Cu in Pernatty Lagoon, both Zn and Pb follow a weak but distinct relationship with εNd similar to what was seen in Moola or Olympic Dam, where metal content increased with a more positive εNd. This indicates that Nd, Pb and Zn all originate from the same fluid source whereas Cu most likely does not.

Trace Elements and interpretation

The use of Co:Ni ratios to determine the origin (hydrothermal, sedimentary, magmatic, submarine exhalative) of ore formation has seen prevalent use in the past (Bajwah et al., 1987; Gavelin and Gabrielson, 1947; Loftus-Hills and Solomon, 1967; Monteiro et al., 2008). Figure 19 above shows the correlation between Co and Ni in SAR8. Most Co:Ni ratios lie between 0.1 and 10, and appear to group into two distinct areas, indicating sedimentary and hydrothermal input into copper mineralisation. The trace metal ratios were obtained from garnets, which are inferred to be synchronous to mineralisation and thus their chemistry was used to model metal deposition. Typically, pyrite is used to interpret such values, however in this case garnets were proxied.

Backscatter electron microscope images (Figure 14) show textural relationships between garnets and other minerals at various depths in SAR8. As can be seen in garnet 90, sulphides appear as inclusions within the garnet, as well as overgrowing the rim. This indicates two interrupted stages of sulphide crystallisation. Another potential example of two stages of sulphur crystallisation can be seen in Figure 2, in which Cu is decoupled form Pb and Zn as a function of depth. There are no observed structural isolators between the areas of mineralised Cu, Zn and Pb.

Due to the atomic structure of garnets ($X_3Y_2Z_3O_{12}$) trace elements can substitute into the lattice, replacing various cations X, or Y, but rarely Z which typically exists as Si (Smith et al., 2004). Various different mechanisms exist for the substitution and insertion of elements into the structure of garnets. YAG type coupled substitution is most commonly seen in the garnet skarns at Pernatty Lagoon in which charge imbalances within the garnet X, Y or Y site are substituted by other elements with a different ionic charge. This YAG substitution is the primary reason for the segregation of LREE and HREE, in which LREE favourable occur in Fe–rich, andradite garnets, and HREE occur in more Al rich, grossular-like garnets (Figure 13). This trend however does not correlate to the anatomy of the garnet, as the cores and rims are not compositionally exclusive and often sporadically comprise of Al and Fe (Table 5).
The acidity of the fluid within a mineralising system can be determined based off the La/Lu ratio compared to Eu (Bau, 1991). When correlated to Eu, a La:Lu >1 indicates a fluid under acidic conditions, which allows for Eu sorption and in turn generates a positive Eu Anomaly as can be seen Figures 16 and 17. Contrastingly a La:Lu<1 equates to more neutral to basic fluid compositions. Figure 13 indicates the fluid at Pernatty Lagoon was mostly acidic, as values of La:Lu are generally >1. These correspond to the Eu anomalies in seen in Figures 16 and 17, however there is no relationship between Eu and mineralisation, as positive Eu anomalies occur in strongly and weakly mineralised regions of SAR8. The Eu anomalies seen at Pernatty Lagoon are inconsistent with those at Hillside and Punt Hill with Eu enrichment in Fe garnet and no Eu anomalism respectively (Nikolakopolous, 2013), indicating Eu is defined by more local geochemical activities than regional.

Typically fluids in the Olympic Dam IOCG region contain fluorine, chlorine or hydroxide complexes which mobilise REEs (Bastrakov et al., 2007). Fluorine increases the solubility of HREEs, hence the relative depletion we see at Pernatty Lagoon (Agangi et al., 2010). Furthermore, fluorine complexes play an instrumental role in REE transport through the IOCG province in the Gawler Craton (Manning, 2012; McPhie et al., 2012; Migdisov et al., 2009) The presence of large fluorite crystals in skarn at Pernatty Lagoon further indicates the presence of F containing fluids.

Aside from REES, the enrichment or depletion of other trace elements is indicative of fluid composition and precipitation conditions in a system. Of trace elements, Pernatty Lagoon is relatively enriched with Sn, W and As (Figure 20). Despite this relative enrichment there is no relationship between trace element enrichment and mineralisation, indicating that the two were emplaced in separate events, or the trace elements were remobilised. Enrichment of As however is indicative of granitic fluid nature (Verdugo Ihl et al., 2017), which supports the running theory that the HIS played a role in mineralisation.

Relative enrichment of LREEs indicates the skarn in Pernatty Lagoon is retrograde. It is likely that the prograde skarn was replaced or obliterated through metasomatism or other fluid related processes. This provides further evidence for the HIS fluid source in Pernatty Lagoon, as commonly LREES are enriched relative to HREEs in magmatic fluids (Flynn and Wayne Burnham, 1978). LREE enrichment within skarns and IOCG deposits in garnet rims provides evidence for changing salinity conditions from high to low.

CONCLUSIONS

- HIS or GRV interaction with pre-existing metasediments in Pernatty were likely responsible for the mineralisation of Cu, Zn and Pb.
- The εNd of Pernatty Lagoon indicates a crustal evolved source of mineralisation with potential minor mantle components. The isotopic composition of the HIS and Wallaroo group infer that interaction between the two generated the mineralised horizon in Pernatty Lagoon
- The relative enrichment of LREEs compared to HREEs in Pernatty Lagoon strongly suggests that at least one of the fluids that travelled through the system was fluorine rich.
- REE data also suggests fluid was compositionally saline and acidic, and likely to be of similar composition to that of Olympic Dam as it also favours oxidised granites to precipitate copper.
- Co:Ni ratios support the notion that the HIS was instrumental in Pernatty Lagoon mineralisation, as the ratios between the two are indicative of hydrothermal fluid input, which was likely to have been derived from the HIS. Sedimentary input into garnet formation and therefore mineralisation is likely to have occurred from pre-existing sediments.
- The mineralisation seen at Pernatty Lagoon was unlikely to be of the same source as Olympic Dam due to key isotopic differences, however the mineralisation at Pernatty Lagoon is likely to be syngenetic to that of Punt Hill.
- Further isotopic and trace element analysis on individual minerals such as chalcopyrite, zinc, and galena in future would provide more accurate results and definitively conclude the origin of metals in Pernatty Lagoon. Unfortunately,

due to time constraints individual mineral analysis was not within the scope of this study.

- Further sampling of other drillholes in Pernatty Lagoon would assist in constructing an atlas-style map of mineralisation in the Stuart Shelf.

ACKNOWLEDGMENTS

Firstly, I would like to thank my supervisor Prof Martin Hand, for extending this unique opportunity to conduct research in the area of my interest. His insights, encouragement and guidance were invaluable. I would like to thank Dr Alec Walsh for his support and guidance throughout the year. I would also like to thank David Bruce and Sarah Gilbert from the University of Adelaide and Adelaide microscopy respectively for going above and beyond in helping me obtain my data. Many thanks also go to the staff at Tonsley Drillcore Library. Finally, I would like to thank my family and friends, especially Cameron Macphail and Mitchell Bockmann, for all their help, encouragement, support, guidance and insight.

REFERENCES

. *Mineralogical Magazine* (Vol. 81).

AGANGI, A., KAMENETSKY, V. S., & MCPHIE, J. (2010). The role of fluorine in the concentration and transport of lithophile trace elements in felsic magmas: Insights from the Gawler Range Volcanics, South Australia. *Chemical Geology, 273*(3–4), 314-325. doi:https://doi.org/10.1016/j.chemgeo.2010.03.008

BAJWAH, Z. U., SECCOMBE, P. K., & OFFLER, R. (1987). Trace element distribution, Co:Ni ratios and genesis of the big cadia iron-copper deposit, new south wales, australia. *Mineralium Deposita, 22*(4), 292-300. doi:10.1007/BF00204522

BASTRAKOV, E. N., SKIRROW, R. G., & DAVIDSON, G. J. (2007). Fluid evolution and origins of iron oxide Cu-Au prospects in the Olympic Dam district, Gawler Craton, South Australia. *Economic Geology, 102*(8), 1415-1440.

BAU, M. (1991). Rare-earth element mobility during hydrothermal and metamorphic fluid-rock interaction and the significance of the oxidation state of europium. *Chemical Geology, 93*(3), 219-230. doi:https://doi.org/10.1016/0009-2541(91)90115-8

CAVE, B. (2010). *Copper-Gold Expoloration in the Middleback Ranges; Source(s) of Fluids and Metals*, (Unpublished honours thesis) The University of Adelaide, Australia.

CIOBANU, C. L., WADE, B. P., COOK, N. J., MUMM, A. S., & GILES, D. (2013). Uranium-bearing hematite from the Olympic Dam Cu–U–Au deposit, South Australia: A geochemical tracer and reconnaissance Pb–Pb geochronometer. *Precambrian Research, 238*, 129-147.

CONOR, C., RAYMOND, O., BAKER, T., TEALE, G., SAY, P., & LOWE, G. (2010). *Alteration and mineralisation in the Moonta-Wallaroo Cu-Au mining field region, Olympic Domain, South Australia* (Vol. 3).

FABRIS, A., KATONA*, L., REED, G., KEEPING, T., GORDON, G., GOUTHAS, G., & SWAIN, G. (2016). *Mapping the Punt Hill IOCG system using geophysical, geochemical and spectral methods–an integrated approach.* Paper presented at the ASEG Extended Abstracts 2016: 25th International Geophysical Conference and Exhibition.

FLYNN, R. T., & WAYNE BURNHAM, C. (1978). An experimental determination of rare earth partition coefficients between a chloride containing vapor phase and silicate melts. *Geochimica et Cosmochimica Acta, 42*(6), 685-701. doi:https://doi.org/10.1016/0016-7037(78)90087-X

GAVELIN, S., & GABRIELSON, O. E. (1947). *Spectrochemical investigations of sulphide minerals from the ores of the Skellefte District. On the significance of minor constituents for certain practical and theoretical problems in economic geology*. Stockholm: P.A. Norstedt.

GLEASON, J. D., MARIKOS, M. A., BARTON, M. D., & JOHNSON, D. A. (2000). Neodymium isotopic study of rare earth element sources and mobility in hydrothermal Fe oxide (Fe-P-REE) systems. *Geochimica et Cosmochimica Acta, 64*(6), 1059-1068. doi:https://doi.org/10.1016/S0016-7037(99)00325-7

GOLDSTEIN, S., K. ONIONS, R., & HAMILTON, J. (1984). *Goldstein, S. L. , O'Nions, R. K. & Hamilton, P. J. A Sm-Nd isotopic study of atmospheric dusts and particulates from major river systems. Earth Planet. Sci. Lett. 70, 221-236* (Vol. 70).

HAND, M., REID, A., & JAGODZINSKI, L. (2007). Tectonic framework and evolution of the Gawler craton, southern Australia. *Economic Geology, 102*(8), 1377-1395.

HITZMAN, M. W., ORESKES, N., & EINAUDI, M. T. (1992). Geological characteristics and tectonic setting of proterozoic iron oxide (Cu□U□Au□REE) deposits. *Precambrian Research, 58*(1), 241-287. doi:https://doi.org/10.1016/0301-9268(92)90121-4

HOWARD, K. E., HAND, M., BAROVICH, K. M., REID, A., WADE, B. P., & BELOUSOVA, E. A. (2009). Detrital zircon ages: Improving interpretation via Nd and Hf isotopic data. *Chemical Geology, 262*(3), 277-292. doi:https://doi.org/10.1016/j.chemgeo.2009.01.029

ISMAIL, R., CIOBANU, C. L., COOK, N. J., TEALE, G. S., GILES, D., MUMM, A. S., & WADE, B. (2014). Rare earths and other trace elements in minerals from skarn assemblages, Hillside iron oxide–copper–gold deposit, Yorke Peninsula, South Australia. *Lithos, 184*(Supplement C), 456-477. doi:https://doi.org/10.1016/j.lithos.2013.07.023

JOHNSON, J. (1993). *The Geochronology and radiogenic isotope sustematics of the Olympic Dam Copper-Uranium-Gold-Silver deposit, South Australia*, (Unpublished Doctoral Thesis) The Australian National University, Australia.

JOHNSON, J., & MCCULLOCH, M. (1995). *Sources of mineralising fluids for the Olympic Dam deposit (South Australia): Sm--Nd istopic constraints* (Vol. 121).

LOFTUS-HILLS, G., & SOLOMON, M. (1967). Cobalt, nickel and selenium in sulphides as indicators of ore genesis. *Mineralium Deposita, 2*(3), 228-242. doi:10.1007/BF00201918

MANNING, D. A. C. (2012). The fluorine link between a supergiant ore deposit and a silicic large igneous province: COMMENT. *Geology, 40*(8), e275-e275. doi:10.1130/G33040C.1

MASON, M., SIMPSON, P., UREN, B., PEDLER, A., & DUNBAR, G. (1983). Red Lake. Progress reports for the period 23/2/1978 to 2/1/1983. *Open file Envelope, 03245*.

MCPHIE, J., KAMENETSKY, V., ALLEN, S., EHRIG, K., AGANGI, A., & BATH, A. (2012). The fluorine link between a supergiant ore deposit and a silicic large igneous province: REPLY. *Geology, 40*(8), e276-e276. doi:10.1130/G33378Y.1

MIGDISOV, A. A., WILLIAMS-JONES, A. E., & WAGNER, T. (2009). An experimental study of the solubility and speciation of the Rare Earth Elements (III) in fluoride- and chloride-bearing aqueous solutions at temperatures up to 300°C. *Geochimica et Cosmochimica Acta, 73*(23), 7087-7109. doi:https://doi.org/10.1016/j.gca.2009.08.023

MONTEIRO, L. V. S., XAVIER, R. P., DE CARVALHO, E. R., HITZMAN, M. W., JOHNSON, C. A., DE SOUZA FILHO, C. R., & TORRESI, I. (2008). Spatial and temporal zoning of hydrothermal alteration and mineralization in the Sossego iron oxide–copper–gold deposit, Carajás Mineral Province, Brazil: paragenesis and stable isotope constraints. *Mineralium Deposita, 43*(2), 129-159. doi:10.1007/s00126-006-0121-3

NEBEL, O., NEBEL-JACOBSEN, Y., MEZGER, K., & BERNDT, J. (2007). Initial Hf isotope compositions in magmatic zircon from early Proterozoic rocks from the Gawler Craton, Australia: A test for zircon model ages. *Chemical Geology, 241*(1), 23-37. doi:https://doi.org/10.1016/j.chemgeo.2007.02.008

NIKOLAKOPOLOUS, D. (2013). *Ore vectoring in IOCG systems: trace elements in garnets from the Groundhog skarn, Punt Hill, South Australia*, (Unpublished honours thesis) The University of Adelaide, Australia.

REID, A., & FABRIS, A. (2015). Influence of preexisting low metamorphic grade sedimentary successions on the distribution of iron oxide copper-gold mineralization in the Olympic Cu-Au province, Gawler craton. *Economic Geology, 110*(8), 2147-2157.

REID, A., FLINT, R., MAAS, R., HOWARD, K., & BELOUSOVA, E. (2009). Geochronological and isotopic constraints on Palaeoproterozoic skarn base metal mineralisation in the central Gawler Craton, South Australia. *Ore Geology Reviews, 36*(4), 350-362.

REID, A., SWAIN, G., MASON, D., & MAAS, R. (2011). Nature and timing of Cu-Au-Zn-Pb mineralisation at Punt Hill, eastern Gawler Craton. *MESA Journal, 60*, 7-17.

SCHLEGEL, T. U., & HEINRICH, C. A. (2015). Lithology and hydrothermal alteration control the distribution of copper grade in the Prominent Hill iron oxide-copper-gold deposit (Gawler craton, South Australia). *Economic Geology, 110*(8), 1953-1994.

SCHWARTZ, S. (2010). *An investigation into the hydrothermal fluids associated with alteration of a metasedimentary-hosted IOCG system in the Eastern Gawler Craton*, (Unpublished honours thesis) Macquarie University, Australia.

SIPAHI, F., AKPINAR, İ., EKER, Ç. S., KAYGUSUZ, A., VURAL, A., & YILMAZ, M. (2017). Formation of the Eğrikar (Gümüşhane) Fe–Cu skarn type mineralization in NE Turkey: U–Pb zircon age, lithogeochemistry, mineral chemistry, fluid inclusion, and O-H-C-S isotopic compositions. *Journal of Geochemical Exploration, 182*(Part A), 32-52. doi:https://doi.org/10.1016/j.gexplo.2017.08.006

SKIRROW, R. G., BASTRAKOV, E. N., BAROVICH, K., FRASER, G. L., CREASER, R. A., FANNING, C. M., . . . DAVIDSON, G. J. (2007). Timing of iron oxide Cu-Au-(U) hydrothermal activity and Nd isotope constraints on metal sources in the Gawler craton, South Australia. *Economic Geology, 102*(8), 1441-1470.

SKIRROW, R. G., & DAVIDSON, G. J. (2007). A special issue devoted to Proterozoic iron oxide Cu-Au-(U) and gold mineral systems of the Gawler Craton: preface. *Economic Geology, 102*(8), 1373-1375.

SMITH, M. P., HENDERSON, P., JEFFRIES, T. E. R., LONG, J., & WILLIAMS, C. T. (2004). The Rare Earth Elements and Uranium in Garnets from the Beinn an Dubhaich Aureole, Skye, Scotland, UK: Constraints on Processes in a Dynamic Hydrothermal System. *Journal of Petrology, 45*(3), 457-484. doi:10.1093/petrology/egg087

VERDUGO IHL, M., CIOBANU, C., COOK, N., COURTNEY-DAVIES, L., EHRIG, K., & GILBERT, S. (2017). *Trace element signatures in U-W-Sn-Mo zoned hematite from the IOCG deposit at Olympic Dam, South Australia*.

WILKINSON, J. J., JENKIN, G. R. T., FALLICK, A. E., & FOSTER, R. P. (1995). Oxygen and hydrogen isotopic evolution of Variscan crustal fluids, south Cornwall, U.K.

Chemical Geology, 123(1), 239-254. doi:https://doi.org/10.1016/0009-2541(95)00053-O

APPENDIX A

SAMPLING STRATEGY AND SARIG

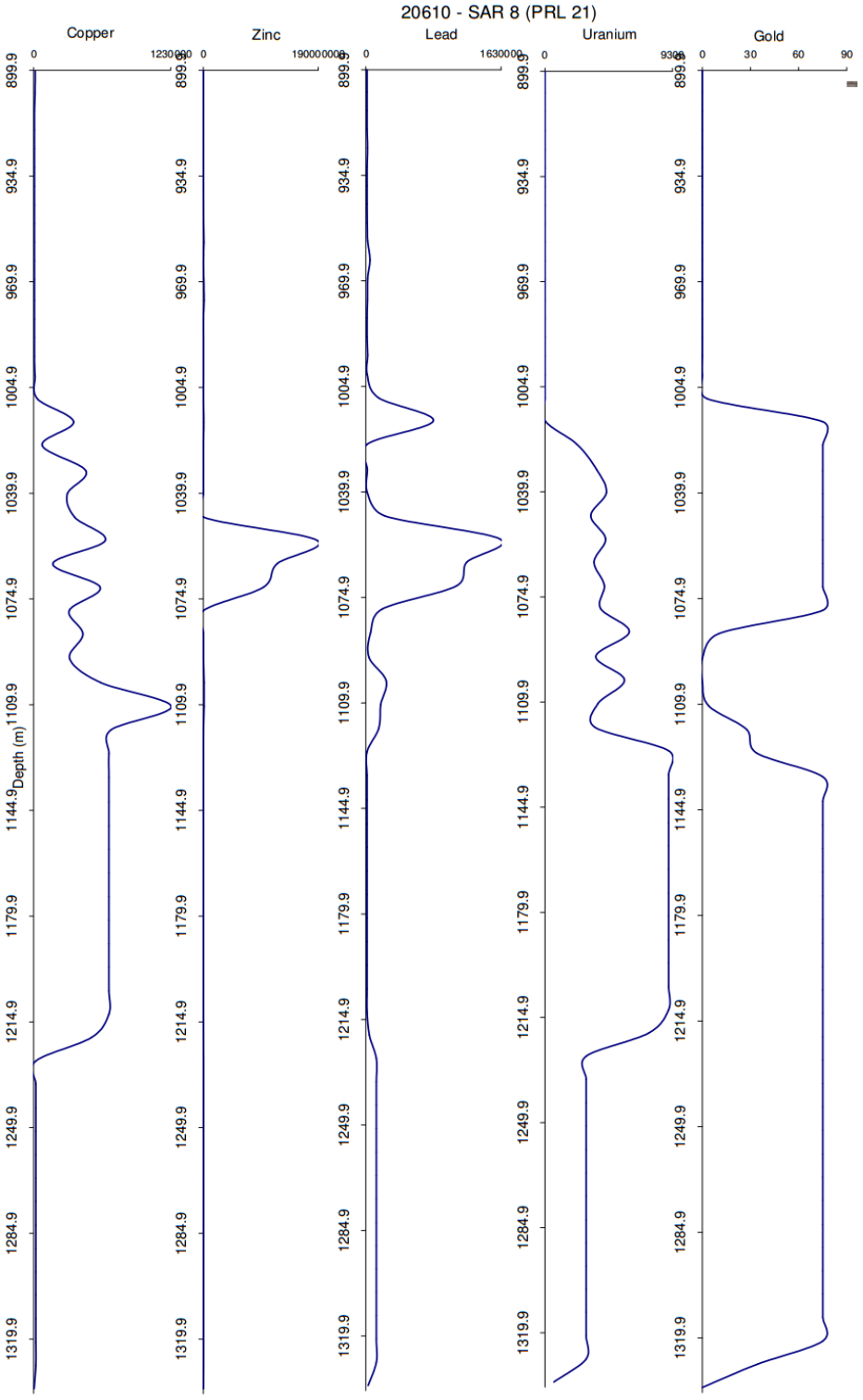

Figure A 1: Hylogger data from SARIG showing metal abundance as a function of depth in SAR8

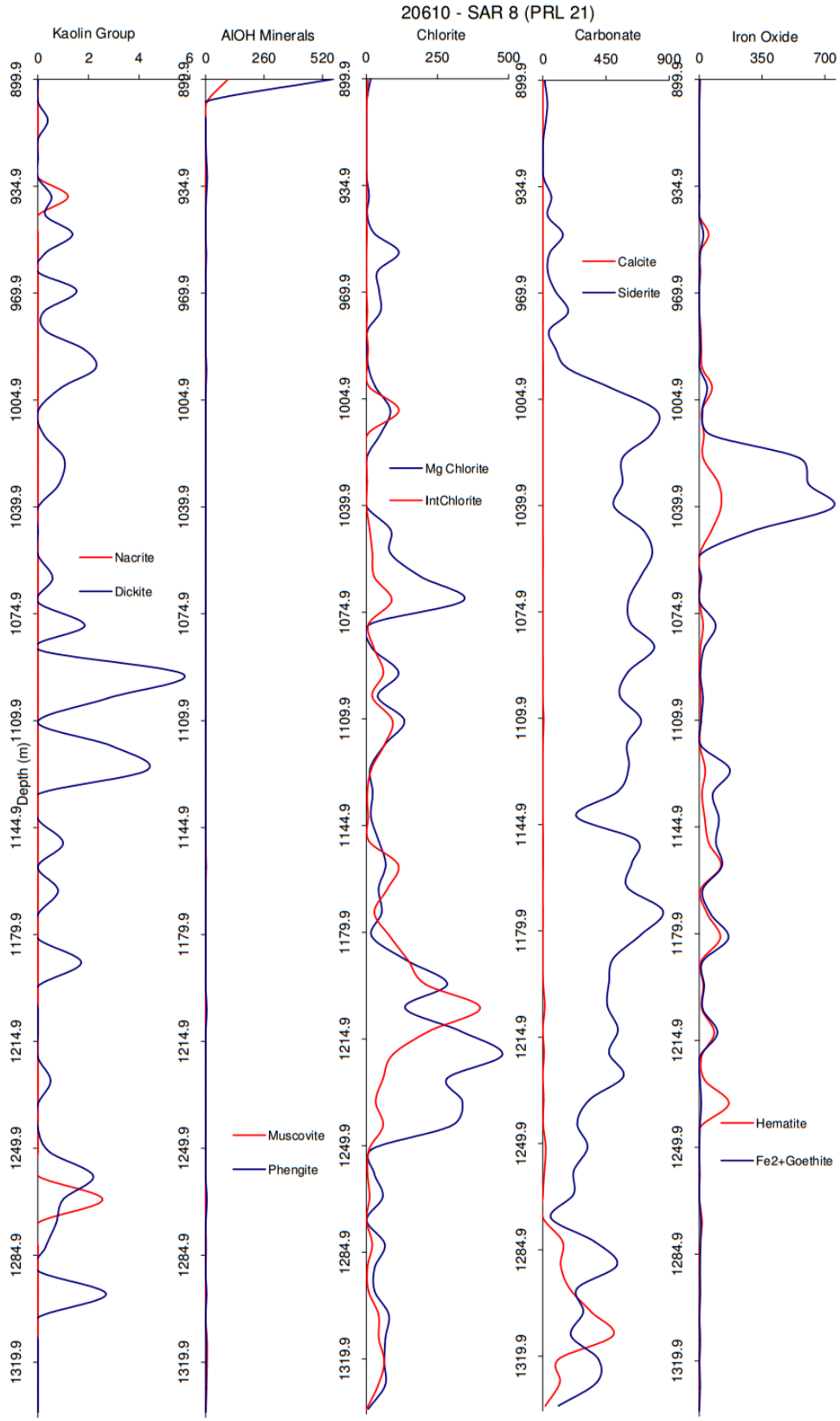

Figure A 2: Hylogger data from SARIG showing mineral abundance in SAR8 used to determine altered and unaltered zones.

Table A 1: SARIG geochemical data for SAR8 collected by Fabris (2012).

Depth Interval (m)	SiO_2	Al_2O_3	CaO	Fe_2O_3	K_2O	MgO	MnO	Na_2O	P_2O_5	TiO_2	Ag	As	Au	Ba	Be	Bi	Cd	Ce	Co	Cr	Cs	Cu	Dy
	%	%	%	%	%	%	%	%	%	%	ppm	ppm	ppb	ppm	ppm	ppm	ppm	ppm	ppm	ppm	ppm	ppm	ppm
369.5-370.4	66.09	12.98	0.56	5.36	6.5	1.06	0.17	1.56	0.14	0.65	0.11	8.7	1	1056.8	2.5	0.91	0.02	213.1	9.8	20	5.82	11	9
410.1-411.1	64.25	12.52	1.05	6.04	6.96	1.48	0.33	0.43	0.16	0.66	0.13	6.3	1	865.9	2.9	0.88	0.02	196.9	9.4	20	8.39	9	8.58
449-450	66.35	12.93	0.98	6.7	6.8	1.42	0.3	0.58	0.11	0.65	0.1	3.6	1	1070.4	2.7	0.62	0.02	176	13.4	20	7.87	7	8.15
489.5-490.5	64.74	12.73	1.09	5.82	6.85	1.25	0.18	1.17	0.15	0.66	0.09	3.4	1	1156	2.6	0.8	0.02	197.7	8.8	23	5.31	7	8.15
529.8-530.8	64.03	12.72	1.24	5.48	6.42	1.49	0.2	1.76	0.14	0.65	0.1	4.2	1	1282.2	2.7	0.62	0.02	179.9	9.4	20	3.48	7	8.11
568.8-569.8	65.44	12.77	1.45	6.53	7.09	1.61	0.38	0.36	0.15	0.67	0.08	6.7	1	1303.6	2.7	0.31	0.02	176.7	14.1	20	6.7	8	8.01
586.35-587	56.05	13.32	2.39	8.31	9.89	1.31	0.47	0.26	0.15	0.69	0.1	25.8	1	1920.4	1.9	4.02	0.02	357.3	7.2	20	3.98	7	10.29
610.9-611.9	76.55	11.09	0.23	3.95	5.12	0.35	0.07	0.15	0.03	0.43	0.06	9.5	1	543.4	2.4	0.24	0.05	175.5	2	27	9.32	6	6.06
659.5-650.4	73.28	12.09	0.39	2.61	6.37	0.53	0.11	0.17	0.03	0.25	0.06	4	1	638.6	2.9	0.3	0.02	100.4	2.8	20	5.49	9	9.88
690.65-691.65	70.5	11.7	0.43	3.62	8.09	0.48	0.07	0.18	0.03	0.24	0.23	5.2	1	1184.2	2.5	0.7	0.05	205.3	2.6	20	3.68	7	11.65
730.2-731.2	65.27	14.88	0.79	4.45	7.94	0.8	0.13	0.86	0.15	0.61	0.17	1.7	1	2291.5	2.4	9.65	0.02	146.4	6.7	20	3.74	411	7.4
810.4-811.4	63.73	14.63	1.07	5.23	5.55	1.15	0.12	2.92	0.11	0.45	0.06	2.3	1	1792.3	1.7	0.07	0.02	102.7	4.1	43	3.34	18	3.7
849.1-850.1	64.44	14.28	1.15	3.83	5.62	1.1	0.11	2.81	0.09	0.4	0.05	2	1	2400.4	1.8	0.08	0.02	81.4	3.2	45	3.17	7	3.05
889.15-890.15	61.42	13.95	0.94	5.04	6.06	1.18	0.08	2.57	0.08	0.43	0.09	4.6	1	2688.7	1.9	0.22	0.02	72.3	6.5	49	2.92	10	2.89
905.1-906.1	63.9	14.48	1.74	5.09	4.28	1.85	0.13	1.85	0.1	0.4	0.09	4.4	3	1520.7	3.6	0.17	0.02	87.7	11.7	39	8.77	33	3.16
906.3-908.1	57.07	17.3	1.15	6.95	2.36	1.04	0.09	6.4	0.03	0.59	0.18	2.4	1	803.5	2.4	0.2	0.02	49	6	73	7.45	24	4.58
917.7-918.7	50.78	10.58	1.31	22.1	4.26	0.71	0.12	2.93	0.15	0.41	0.05	5.2	1	6055.3	0.8	0.06	0.02	16.4	4.3	62	0.87	7	1.9
929.6-930.6	49.17	10.74	3.11	18.11	4.35	2.38	0.37	2.16	0.2	0.42	0.3	14.8	1	6638	3.5	1.36	0.22	350.5	9	63	1.56	16	6.37
939.3-940.3	49.14	12.8	3.21	17.56	1.37	1.62	0.15	6.37	0.3	0.44	0.12	7.4	1	8429.1	1.3	0.78	0.09	68.7	5.3	65	0.57	11	3.39
949.2-950.2	48.24	11.5	3.74	15.06	1.35	7.28	1.29	4.7	0.11	0.42	0.25	6.2	1	1568.7	2	4.78	0.02	45.7	19.1	60	0.72	26	2.83
959.85-960.85	52.4	13.02	4.2	9.24	2.56	7.64	1.32	4.66	0.12	0.49	0.1	12.7	1	2287.4	2.3	0.56	0.15	121.4	9.6	62	1.32	14	4.68
970.6-971.6	51.8	12.01	4.13	13.03	8.54	3.65	0.32	1.44	0.1	0.45	0.17	13	2	4547.2	2.5	0.4	0.05	128.1	5.9	63	2.88	12	3.47
979.1-980.1	45.62	12.35	9.93	9.55	5.5	7.78	1.49	0.61	0.11	0.46	0.21	15.6	1	5364.6	2.5	11.99	1.29	98.5	8.4	64	2.27	15	6.19
989.2-990.2	53.43	12.78	4.48	9.78	10.58	4.38	0.28	0.57	0.11	0.5	0.05	11.7	1	4634.1	1.9	0.18	0.02	21.9	9.2	68	4.87	19	3.64
1000.3-1001.3	46.97	10.84	10.04	11.14	6.91	5.51	0.67	0.65	0.13	0.44	0.05	13.8	1	4135.1	1.8	0.21	0.79	221.4	7.5	63	7.51	14	4.53
1010.1 1011.1	48.39	10.78	15.88	7.84	2.73	5.75	0.63	2.06	0.18	0.41	0.95	20.3	1	2110.4	2.7	2.41	0.24	1226.7	13.8	62	3.51	180	3.51
1019.1-1020	51.35	10.64	11.47	7.67	6.95	4.86	0.49	0.77	0.15	0.39	0.19	13.8	1	4169.3	2.2	0.29	1.28	381.2	16.3	56	9.57	152	2.94
1029.3-1030.35	39.38	6.45	19.88	17.91	2.52	2.85	1.17	0.4	0.27	0.24	1.23	171.9	17	1850	1.2	1.73	0.24	41.6	117.6	33	19.28	1394	3.27
1039.1-1040.1	44.32	9.04	14.93	15.6	5.37	2.46	1.06	0.28	0.16	0.34	1.16	102.8	17	4781.8	1.1	1.85	0.14	38.3	81.8	44	15.4	701	3.51
1050.1-1051.1	48.99	10.59	13.23	11.5	7.13	2.37	0.99	0.27	0.15	0.39	1.35	71.6	14	4015.2	2.4	1.12	2.66	24.1	45.9	53	8.68	1164	3.43
1068.3-1069.3	48.63	10.34	10.11	11.04	6.17	3.66	0.76	0.24	0.15	0.41	1.73	143.5	13	4613.4	3.2	1.95	17.94	61.7	48.7	50	2.16	602	2.65

1080.1-1081.1	49.21	10.4	14.83	10.79	7.43	2.09	0.6	0.23	0.09	0.33	1.28	74.7	5	3274.2	2.4	0.93	2.16	162.1	18.3	45	5.49	111	2.99
1089.1-1090.1	50.22	8.92	12.74	9.94	6.46	5.15	0.74	0.34	0.15	0.39	0.73	20.9	2	3730.2	1.8	0.76	0.19	321.6	30.7	48	2.63	130	1.96
1099.2-1100.2	51.44	11.07	10.64	9.6	8.53	3.42	0.59	0.28	0.17	0.44	1.91	106.3	58	4312	1.9	3.16	1.79	34.4	52	56	5.04	2451	2.69
1108.4-1109.4	48.48	12.44	10.65	8.5	8.69	1.69	0.51	0.21	0.09	0.48	0.72	91.5	18	4848	1.8	1.24	0.87	54.2	17.7	64	2.16	334	3.24
1119.25-1120.3	46.41	10.73	12.35	13.73	6.33	2.82	0.66	0.29	0.22	0.34	1.86	106.6	37	3719.8	1.4	1.44	10.19	44.7	39.3	46	5.46	552	3.02
1130.3-1131.3	45.32	9.38	13.1	15.94	5.56	2.95	0.82	0.4	0.25	0.34	3.05	121.8	33	2710.9	1.7	3.11	0.52	93.3	106.1	47	9.96	6417	2.92
1138.8-1139.8	48.34	6.59	15.78	16.42	3.48	2.47	0.77	0.25	0.21	0.2	1.44	134.6	37	1683.2	1.3	2.95	2.34	44.3	76.9	26	10.62	1347	3.14
1148.7-1149.7	41.93	5.36	10.97	25.49	1.91	1.27	0.51	0.3	0.21	0.2	10.54	613.4	162	4266.4	0.8	3.28	0.85	36.9	396.7	31	20.7	17913	2.62
1160.5-1161.45	44.89	10.3	18.47	13.32	5.77	0.93	0.61	0.44	0.11	0.37	0.44	238	7	6068.4	0.9	1.36	1.14	29.3	8.5	55	3.8	52	4.48
1170.85-1171.85	54.86	13.25	8.54	4.99	10.1	2.51	0.33	0.95	0.16	0.53	0.26	28.1	1	5783.2	2.9	0.76	0.6	380.4	22.9	79	2.92	388	3.9
1179.8-1180.8	42.38	10.87	14.43	14.23	5.36	1.91	0.59	0.67	0.26	0.45	3.71	1539.6	41	2790.1	1.5	1.26	12.46	72.4	97.2	62	2.9	750	2.97
1189.2-1190.3	51.36	13.76	9.6	6.33	8.22	4.25	0.4	0.59	0.12	0.53	0.8	18.7	1	4934	2.7	1.65	0.25	370.7	14.2	75	10.6	21	2.06
1201-1202	47.71	13.06	10.14	8.26	7.56	2.29	0.45	1.23	0.13	0.49	2.23	105.2	13	3900.6	1.4	1.54	9.73	372.1	31.1	71	3.24	798	3.1
1209.1-1210.1	48.91	13.61	11.18	9.47	6.97	3.98	0.69	0.91	0.12	0.47	1.33	26.1	2	2833	2.7	0.94	3.57	174.9	15	67	3.29	157	3.68
1218.4-1219.45	50.66	13.32	9.43	9.64	6.94	3.79	0.57	0.82	0.09	0.47	2.11	44.9	3	4312.8	2.1	3.49	3.11	407.8	15.7	71	3.44	78	2.34
1229.1-1230.1	50.27	10.43	13.74	9.64	6.34	5.59	0.57	0.35	0.16	0.33	0.38	58.3	5	2762.5	3.5	0.95	0.35	375.7	14.3	53	3.37	26	2.2
1239.8-1240.8	47.79	11.6	9.11	13.02	5.72	6.95	0.57	0.67	0.07	0.42	0.08	36.7	1	3460.5	1.7	0.58	0.09	77.6	19.5	48	2.34	36	3.95
1249.9-1250.8	43.98	11.07	14.34	15.73	4.82	3.55	0.77	0.28	0.07	0.4	0.31	11.8	1	2227.1	2.8	1.45	0.19	155.2	6.4	39	9.11	12	5.32
1269.3-1270.25	51.79	13.98	8.94	7.98	1.08	3.95	0.77	6.12	0.11	0.5	0.05	7.2	1	948.5	2.5	0.62	0.66	57.3	16.3	60	0.84	12	3.79
1280.3-1281.2	52.41	13.64	5.76	13.18	1.25	2.74	0.26	6.43	0.09	0.48	0.05	6.8	1	1174.1	3.3	0.42	0.2	64.2	12.2	54	0.49	9	3.18
1289.45-1290.45	50.36	10.84	16.16	4.19	5.06	2.45	0.17	1.17	0.03	0.37	0.05	11	1	5594.3	2.2	1.73	0.06	53.9	5.5	56	2.07	11	2.91
1300.7-1301.7	45.83	5.86	22.23	6.29	2.13	2.16	0.2	0.38	0.06	0.18	0.05	5.8	1	1517.9	1.2	0.47	0.02	39.3	5.9	31	1.69	8	1.87
1309.8-1310.8	43.98	9.21	21.89	4.03	3.11	2.33	0.22	1.53	0.04	0.3	0.05	23.7	1	3106	1.4	2.55	0.65	54.2	9.4	41	1.4	38	2.7
1319.6-1320.6	44.08	6.37	22.18	5.86	1.79	2.89	0.29	0.8	0.03	0.17	0.05	5.7	1	3671.6	1.2	0.63	0.02	51.8	6.3	24	1.29	20	2.22
1328.45-1329.4	43.72	6.76	23.07	4.38	2.68	1.25	0.34	0.61	0.06	0.22	0.05	2.5	1	8243.3	1.6	0.12	0.02	36.4	2.6	37	2.7	11	2.87
1336.8-1338	41.81	8.97	23.49	3.28	2.33	1.94	0.36	1.45	0.04	0.31	0.05	4.5	2	3414.4	1.5	1.13	0.22	54	15.5	47	3.8	62	3.1

Depth interval (m)	Er ppm	Eu ppm	F ppm	Ga ppm	Gd ppm	Ge ppm	Hf ppm	Ho ppm	In ppm	La ppm	Li ppm	Lu ppm	Mo ppm	Nb ppm	Nd ppm	Ni ppm	Pb ppm	Pd ppb	Pr ppm	Pt ppb	Rb ppm	Re ppm	S ppm
369.5-370.4	4.9	2.09	948	18.8	9.93	0.27	8.4	1.77	0.08	112.5	32.7	0.68	1	18.56	77.9	1	10	1	22.43	1	322.4	0.002	78
410.1-411.1	4.88	1.89	1037	17.2	9.48	0.49	7.8	1.72	0.096	104.6	38.9	0.67	3.9	18.42	70.2	1	14	1	20.65	1	358.4	0.002	157
449-450	4.61	1.64	1086	18.7	8.73	0.57	8	1.68	0.101	90.3	46.6	0.66	1.5	17.7	65.5	2	9	1	18.69	1	382	0.002	129
489.5-490.5	4.74	1.78	1755	18.5	9.28	0.34	7.8	1.69	0.064	102.2	38.8	0.63	1.7	17.17	72	1	12	1	20.76	1	384.1	0.003	277
529.8-530.8	4.78	1.65	978	18.6	8.74	0.33	7.9	1.7	0.058	91.7	35.5	0.67	1.5	16.68	65.7	3	10	1	18.88	1	351.3	0.002	191
568.8-569.8	4.72	1.91	1215	18.2	8.97	0.44	7.9	1.67	0.087	90.7	42.1	0.64	1.7	15.93	64.8	4	6	1	18.43	1	425.8	0.003	145
586.35-587	6.17	3.17	947	11.8	12.05	0.29	9.8	2.15	0.072	181.7	16.6	0.97	2.7	14.69	116.5	1	11	1	34.14	1	460.5	0.002	923
610.9-611.9	3.19	2.32	729	16.5	9.12	0.41	6.6	1.14	0.062	96.2	18.6	0.48	0.8	10.7	68.7	4	11	1	19.37	1	354.3	0.002	50
659.5-650.4	6.08	0.92	998	17.9	7.6	0.28	5.1	2.08	0.097	48.5	22.1	0.91	1.7	23.2	36.3	1	9	1	10.82	1	499.6	0.002	64
690.65-691.65	7.43	1.23	802	16.1	11.13	0.22	5.4	2.48	0.037	87.9	14.6	1.11	0.9	24.47	64.4	1	9	1	18.73	1	456.2	0.002	333
730.2-731.2	4.18	1.79	1178	21.1	7.89	0.26	7.2	1.48	0.044	75.2	29.7	0.57	0.6	13.72	55.3	1	6	1	15.5	1	489.5	0.045	581
810.4-811.4	1.92	1.32	1207	19.2	4.71	0.08	4.6	0.7	0.035	55.1	35.2	0.28	0.7	8.42	38.8	27	6	1	10.79	1	377.1	0.002	949
849.1-850.1	1.72	0.96	1213	18.6	3.48	0.12	4.4	0.59	0.034	42	31.6	0.23	0.5	9.04	29.1	16	6	1	8.51	1	394.4	0.002	679
889.15-890.15	1.76	0.91	941	16.7	3.38	0.2	4.7	0.6	0.029	37.5	40.3	0.24	1.1	8.72	27.1	17	5	1	7.64	1	355.6	0.003	1271
905.1-906.1	1.85	1.13	1560	18.2	3.9	0.43	4.4	0.65	0.063	46.7	76.4	0.27	0.7	10.25	31.7	19	5	1	9.19	1	409.4	0.002	187
906.3-908.1	2.99	0.8	1425	23.8	3.63	0.83	3.2	0.98	0.044	24.6	47.9	0.45	0.5	9.76	19.2	25	5	1	5.33	2	214.6	0.002	206
917.7-918.7	1.13	0.44	386	15.3	1.91	0.76	2	0.38	0.016	7.8	19	0.17	0.1	9.57	7.6	23	5	1	1.88	1	167.4	0.002	1328
929.6-930.6	2.81	2.5	4622	15.6	9.19	1.32	2.3	1.15	0.103	214.8	99	0.26	0.1	12.42	97	20	52	1	32	1	211.7	0.002	1406
939.3-940.3	1.86	1.03	1327	16.7	4.61	0.79	2.5	0.69	0.023	34.6	22.7	0.21	0.1	8.6	28.1	8	15	2	7.46	1	71.9	0.003	2075
949.2-950.2	1.64	0.57	3172	19.5	2.96	0.98	2.6	0.59	0.046	23.1	77.9	0.18	0.1	9.4	18.3	37	41	1	4.88	1	79	0.002	293
959.85-960.85	2.63	1.39	1380	23.2	5.84	0.89	2.7	0.92	0.07	63.9	128.5	0.31	0.1	11.87	45.2	30	31	2	12.67	1	125.6	0.002	341
970.6-971.6	1.93	1.15	1439	15	4.63	0.97	2.7	0.7	0.022	69.9	24.6	0.24	0.1	10.77	43.7	20	45	1	12.65	1	397.3	0.002	406
979.1-980.1	3.07	2.15	1813	22.9	6.72	1.42	2.7	1.18	0.284	52.8	69.5	0.28	0.1	13.58	37.5	21	60	2	10.24	1	308.9	0.002	949
989.2-990.2	1.97	0.76	3894	13.9	3.67	0.88	3	0.74	0.031	9.5	29.9	0.19	0.1	13.39	12.6	21	6	2	2.83	1	459.7	0.002	441
1000.3-1001.3	2.2	3.38	1270	15.7	6.53	1.15	2.5	0.85	0.149	129.7	47.9	0.2	0.1	11.96	74.2	20	46	1	22.69	1	356.2	0.002	841
1010.1 1011.1	2.08	2.97	1646	12.7	6.8	1.14	2.5	0.71	0.245	716.7	35.4	0.29	0.1	10.06	319.2	7	243	1	116.32	1	144.3	0.002	1737
1019.1-1020	1.6	0.74	705	9.4	3.4	0.73	2.1	0.58	0.133	211.8	32.3	0.16	0.1	10.59	96.3	14	218	1	35.63	1	365.2	0.002	1422
1029.3-1030.35	1.77	1.55	3367	15.6	4.35	0.94	1.5	0.66	0.547	12.6	22.8	0.17	1.3	9.33	29.5	21	169	1	6.31	1	161.8	0.003	16777
1039.1-1040.1	1.75	1.16	2318	16.7	4.8	0.91	2.4	0.67	0.342	17.5	28.6	0.18	4.2	10.56	21.5	19	49	1	4.75	1	282.1	0.003	15140
1050.1-1051.1	1.91	0.98	3360	14.2	4.11	0.89	2.3	0.69	0.262	9.8	26.7	0.2	10	11.54	17	15	176	1	3.39	1	322	0.002	6155
1068.3-1069.3	1.52	0.74	1482	13.1	2.94	0.91	2.6	0.52	0.259	32.1	59.3	0.15	0.8	11.4	21.4	17	1627	1	6.29	1	251.4	0.003	8783
1080.1-1081.1	1.64	1.01	2686	12.7	3.74	1.01	2.6	0.58	0.216	92.4	16	0.17	1.8	9.42	43.3	10	172	1	14.99	1	344.4	0.008	1685

1089.1-1090.1	1.14	0.68	812	10.5	2.36	0.91	2.8	0.41	0.277	186.1	32	0.12	1.8	12.07	76.4	9	49	1	28.55	1	315.7	0.003	1643
1099.2-1100.2	1.56	0.73	1504	11.5	2.84	0.82	3.1	0.54	0.226	17.9	28.5	0.88	2.8	14.1	14.8	24	64	1	3.81	1	384.2	0.004	7687
1108.4-1109.4	1.73	0.79	1293	18.2	3.63	0.63	3.2	0.66	0.176	26.2	30.7	0.19	0.7	13.63	21.5	12	60	1	5.87	1	360.6	0.002	3027
1119.25-1120.3	1.71	1.08	2638	18.4	3.14	0.8	2.4	0.6	0.406	19.1	33.2	0.15	2.3	11.07	22.4	13	1140	1	5.55	1	283.3	0.005	6880
1130.3-1131.3	1.61	1.13	2306	13.2	3.49	0.87	2.5	0.58	0.491	50.3	27.2	0.15	7.8	10.76	31.4	70	80	1	9.54	1	282.7	0.003	18814
1138.8-1139.8	1.6	1.47	5643	11.3	3.73	0.8	2.2	0.59	0.489	14.6	25.5	0.15	3.4	7.56	29.2	38	406	1	6.48	1	196.6	0.002	11264
1148.7-1149.7	1.33	1.08	6738	12.8	4.03	0.87	3	0.5	0.956	15.7	21.5	0.13	57.6	11.86	21.2	206	84	3	4.73	1	159.6	0.048	89800
1160.5-1161.45	2.13	1.37	1267	14.4	6.1	0.8	2.2	0.82	0.189	12.1	13.8	0.25	4.9	10.81	19.7	1	137	1	3.93	1	271.4	0.002	2544
1170.85-1171.85	2.14	1.4	673	12.4	5.04	0.8	3	0.79	0.101	219.3	20.8	0.23	1.8	12.7	100.3	15	31	2	35.51	1	448.4	0.002	1548
1179.8-1180.8	1.65	1.4	1656	18.9	4.3	0.78	2.6	0.59	0.417	38.3	42.1	0.18	27.3	14.21	27.5	16	1062	14	7.74	2	311.3	0.002	15808
1189.2-1190.3	1.32	0.88	931	14.2	3.03	0.69	2.8	0.43	0.13	214.6	52.7	0.15	1	13.3	93.7	19	91	1	34.26	1	464.6	0.002	598
1201-1202	1.85	1.18	996	13.8	3.82	0.64	2.8	0.65	0.213	221.1	38.9	0.2	2.6	12.65	91.5	12	1394	2	34.64	1	390.9	0.002	5573
1209.1-1210.1	2.1	0.96	1364	17.9	4.08	0.8	3.1	0.73	0.187	97.1	59.3	0.28	63.1	12.88	45	10	335	1	16.07	1	370.9	0.033	1839
1218.4-1219.45	1.53	1.13	1377	17.6	3.58	0.88	2.7	0.49	0.236	230	64	0.17	23	11.22	106.1	8	1522	1	37.61	1	333.8	0.024	2461
1229.1-1230.1	1.14	1.84	2798	14.7	3.54	1.08	2.2	0.4	0.307	209.6	35.1	0.1	0.1	7.04	101.1	15	254	1	35.3	1	315	0.003	2779
1239.8-1240.8	1.95	2.41	3534	18.2	5.03	1	2.4	0.74	0.469	40.2	77	0.21	0.1	10.2	30.4	24	39	1	8.23	1	251.3	0.002	2991
1249.9-1250.8	2.91	1.99	2456	20	6.24	1.38	2.6	1.07	0.348	90	40.7	0.34	0.1	9.54	51.7	14	66	1	15.08	1	252.1	0.002	1035
1269.3-1270.25	2.12	0.95	2267	19.4	4.23	0.85	2.8	0.78	0.038	27.6	47.9	0.22	0.2	12.3	23.8	30	53	2	6.13	2	57.6	0.002	823
1280.3-1281.2	1.85	0.86	1744	18.7	3.83	0.96	2.7	0.64	0.034	32.2	25.3	0.22	0.1	12.57	25.9	26	31	3	6.82	1	65.6	0.002	1052
1289.45-1290.45	1.65	0.81	1566	13.9	3.41	0.92	2.7	0.61	0.083	27.6	20.5	0.17	0.1	10.35	22.2	13	32	1	5.93	1	259.1	0.002	1953
1300.7-1301.7	1.1	0.43	1439	8.6	2.27	0.69	1.7	0.38	0.029	19.7	39.5	0.11	0.1	5.57	15.8	12	7	1	4.32	1	165.4	0.002	1800
1309.8-1310.8	1.53	0.73	1351	11.8	3.39	0.61	2.8	0.56	0.057	27.2	15.9	0.17	0.6	7.53	21.5	8	14	1	5.93	1	192.7	0.002	2252
1319.6-1320.6	1.2	0.77	1236	8.9	2.94	0.96	2.4	0.45	0.04	26.5	31.8	0.18	1.5	5.26	20.3	3	5	1	5.58	1	104.4	0.002	1895
1328.45-1329.4	1.42	0.72	445	8.5	3.2	0.73	1.8	0.56	0.046	17.3	24.7	0.12	0.1	5.82	16.2	6	5	1	4.11	1	162	0.002	1623
1336.8-1338	1.67	0.72	897	11.2	3.55	0.76	2.7	0.63	0.049	26.2	39	0.21	1.1	8.68	22.3	8	36	1	5.82	1	139.5	0.002	2734

Depth interval (m)	Sb ppm	Sc ppm	Se ppm	Sm ppm	Sn ppm	Sr ppm	Ta ppm	Tb ppm	Te ppm	Th ppm	Tl ppm	Tm ppm	U ppm	V ppm	W ppm	Y ppm	Yb ppm	Zn ppm	Zr ppm
369.5-370.4	1.81	12	0.5	13.13	4	39	2.6	1.5	0.05	45.04	2.13	0.75	6.74	52	4	49.3	4.68	81	346
410.1-411.1	2.12	12	0.5	11.82	4	26.4	2.4	1.47	0.05	43.8	3.02	0.76	6.53	51	4	48	4.72	69	331
449-450	1.96	12	0.5	11.14	4	30.9	2.4	1.33	0.05	43.95	2.87	0.71	7.38	57	5	44	4.55	87	328
489.5-490.5	1.6	12	0.5	12.03	4	34.2	2.5	1.41	0.05	45.18	2.84	0.72	6.48	56	5	46.9	4.55	79	311
529.8-530.8	1.28	12	0.5	11.11	4	43.8	2.3	1.35	0.05	43.97	1.75	0.71	6.41	52	3	47.8	4.67	44	329
568.8-569.8	1.86	11	0.7	11.17	4	34.9	2.3	1.35	0.05	42.51	2.5	0.72	5.75	53	4	45.2	4.46	55	327
586.35-587	2.74	10	0.8	17.33	4	56.6	2.6	1.73	0.05	47.5	2.09	0.96	9.3	73	21	64.9	6.18	46	425
610.9-611.9	2.18	9	0.5	12.25	4	16.9	2.2	1.15	0.05	33.86	1.51	0.48	5.29	22	10	32.7	3.16	99	283
659.5-650.4	1.55	8	0.6	7.09	4	18.9	4.5	1.5	0.06	53.94	2.82	0.92	3.9	10	6	59.6	6.17	48	170
690.65-691.65	1.61	8	1	12.39	4	33.3	3.7	1.8	0.05	61.52	1.83	1.18	23.79	10	6	72.7	7.32	43	148
730.2-731.2	1.31	12	0.5	9.68	4	54.7	2.1	1.19	0.05	33.81	1.8	0.61	8.37	54	8	42.6	3.96	46	297
810.4-811.4	1.72	10	0.5	6.36	2	73.7	1.3	0.65	0.05	24.72	1.51	0.29	5.06	70	6	18.9	1.85	58	153
849.1-850.1	1.62	10	0.5	4.74	3	89.2	1.4	0.5	0.05	24.26	1.56	0.26	3.61	53	7	17.3	1.73	47	169
889.15-890.15	1.56	10	0.5	4.39	2	117.9	1.2	0.49	0.05	20.71	1.22	0.26	4.11	68	6	17.3	1.72	51	179
905.1-906.1	2.27	10	0.5	5.19	4	57.6	1.4	0.56	0.05	23.81	1.11	0.28	10.83	53	4	18.9	1.87	42	170
906.3-908.1	1.81	19	0.6	3.8	5	33.4	2	0.69	0.05	17.64	0.57	0.47	6.18	121	10	26.4	2.99	38	110
917.7-918.7	1.48	17	0.5	1.88	3	116.6	1.2	0.31	0.05	11.45	0.86	0.18	1.3	121	4	11.8	1.16	52	62
929.6-930.6	4.63	14	0.5	12.35	3	123.5	1.1	1.3	0.05	11.81	0.79	0.36	2.66	101	7	29.1	2.14	162	69
939.3-940.3	2.37	14	0.5	5.21	4	104	1	0.61	0.09	13.01	0.26	0.27	3.95	119	6	21.3	1.77	171	81
949.2-950.2	1.85	15	0.5	3.39	4	32.4	1.1	0.46	0.05	12.87	0.31	0.24	2.54	113	3	17	1.53	405	81
959.85-960.85	3.93	16	0.5	7.68	4	67.8	1.3	0.82	0.08	15.45	0.78	0.38	3.69	106	3	25.2	2.46	1388	88
970.6-971.6	3.97	15	0.5	6.54	4	66.8	1.1	0.64	0.05	13.59	1.9	0.29	2.28	111	2	19.8	1.83	258	86
979.1-980.1	9.89	16	0.5	7.4	7	576.8	1.4	1.07	0.05	14.33	2.35	0.42	12.31	93	3	31.8	2.46	1840	86
989.2-990.2	2.92	16	0.5	3.76	4	46.8	1.5	0.6	0.05	13.55	2.84	0.29	3.14	102	2	19.7	1.8	72	96
1000.3-1001.3	9.28	15	0.5	10.09	9	301.6	1.2	0.85	0.05	19	2.83	0.32	12.1	97	2	23.4	1.96	752	81
1010.1 1011.1	5.72	14	0.5	18.39	9	138.7	1	0.76	0.05	27.11	1.27	0.31	7.61	128	3	19.6	2.04	273	80
1019.1-1020	2.1	13	0.5	5.91	4	330	1.1	0.49	0.05	10.2	3.86	0.23	3.87	90	3	17.4	1.45	396	67
1029.3-1030.35	9.39	8	2.9	5.9	11	36.4	0.5	0.58	0.22	9.01	2.21	0.25	11.44	64	44	18.2	1.53	142	47
1039.1-1040.1	4.47	9	2.1	5.71	9	61	0.8	0.65	0.19	17.9	3.16	0.26	8.57	59	14	18.7	1.6	114	78
1050.1-1051.1	3.84	11	1.3	4.91	7	46.6	0.9	0.58	0.07	14.09	3.01	0.28	6.3	70	8	19.4	1.71	882	77
1068.3-1069.3	4.32	12	1	3.52	4	78.6	1	0.43	0.06	6.43	1.69	0.21	5.84	51	16	14.9	1.35	5354	85
1080.1-1081.1	2.11	11	0.6	4.93	5	46.3	0.8	0.53	0.05	7.64	2.91	0.24	5.68	65	22	17.5	1.5	736	81

1089.1-1090.1	1.24	11	0.5	4.34	4	78.5	1.1	0.34	0.05	11.18	3.69	0.16	5.66	38	9	11.1	1.08	120	92
1099.2-1100.2	5.56	13	1	3.05	4	45	1.2	0.43	0.12	29.24	3.79	0.24	10.96	53	12	15.5	1.48	722	98
1108.4-1109.4	2.93	15	0.5	4.01	5	91	1.3	0.55	0.05	23.31	2.24	0.26	7.41	66	10	18.1	1.63	355	104
1119.25-1120.3	6.58	11	3.7	3.96	7	73.1	0.8	0.48	0.11	7.36	1.74	0.25	9.79	66	28	18.3	1.51	3373	78
1130.3-1131.3	5.2	11	2.4	4.65	6	38	0.8	0.49	0.29	6.65	3.06	0.23	7.98	53	25	16.3	1.49	247	82
1138.8-1139.8	4.02	6	1.6	5.06	9	32.1	0.5	0.55	0.09	4.84	2.13	0.23	12.02	51	39	16.8	1.39	807	69
1148.7-1149.7	15.29	5	11.3	4.97	11	40.2	0.5	0.5	1.24	15.48	4.12	0.19	10.08	43	17	14.1	1.24	278	102
1160.5-1161.45	3.41	12	0.5	6.55	12	55.9	0.8	0.83	0.05	7.06	2.82	0.32	3.9	113	7	22.6	1.85	299	72
1170.85-1171.85	2.12	15	0.5	8.42	4	130.1	1	0.71	0.05	15.39	3.9	0.32	5.49	94	3	21.3	1.92	163	95
1179.8-1180.8	20.03	12	3.2	5.15	8	107.3	1.1	0.55	0.18	14.51	5.07	0.25	12.18	98	21	16.6	1.65	2894	84
1189.2-1190.3	1.99	17	0.5	6.43	6	385.1	1.3	0.38	0.05	13.18	5.62	0.2	5.87	96	2	11.9	1.32	103	88
1201-1202	4.14	15	1	6.48	7	149.7	1.3	0.54	0.08	16.31	3.97	0.25	11.17	77	9	17.5	1.7	2571	89
1209.1-1210.1	2.93	13	0.5	4.78	5	85.4	1.2	0.62	0.05	13.9	4.07	0.29	8.83	93	4	19.6	1.9	1160	100
1218.4-1219.45	2.55	15	0.5	7.59	8	104.7	1.1	0.45	0.05	18.5	2.37	0.23	13.33	110	8	13.9	1.58	1129	88
1229.1-1230.1	5.1	12	0.5	7.85	18	64.3	0.6	0.42	0.05	13.61	2.74	0.16	7.31	88	3	11.5	1.06	225	72
1239.8-1240.8	6.56	14	0.5	5.74	12	163.2	1	0.73	0.05	12.06	1.62	0.28	18.32	86	2	21.3	1.74	130	78
1249.9-1250.8	6.87	12	0.5	7.76	11	115.9	0.9	0.9	0.05	12.47	1.25	0.42	6.49	84	6	29.1	2.57	130	82
1269.3-1270.25	2.57	17	0.5	4.69	4	74	1.2	0.65	0.05	13.73	0.63	0.31	7.58	99	3	21.1	1.88	546	89
1280.3-1281.2	2.44	16	0.5	4.5	4	84.9	1.2	0.54	0.05	13.55	0.64	0.28	4.06	111	4	18.5	1.77	129	87
1289.45-1290.45	3.63	11	0.5	4.07	3	216.5	1	0.5	0.05	12.19	2.29	0.25	5.96	57	2	16.4	1.54	73	85
1300.7-1301.7	1.42	5	0.5	2.88	1	136.5	0.5	0.33	0.05	7.98	3.57	0.16	2.75	33	2	10.8	1.05	56	56
1309.8-1310.8	1.97	9	0.5	3.97	3	175.8	0.7	0.48	0.05	11.1	2.06	0.22	4.23	39	2	14.9	1.41	159	93
1319.6-1320.6	1.49	4	0.5	3.6	2	172.8	0.4	0.4	0.05	8.54	0.7	0.17	3.76	34	2	12.1	1.06	45	79
1328.45-1329.4	1.24	6	0.5	3.34	2	149.7	0.5	0.49	0.05	7.92	1.2	0.2	2.51	38	2	15.7	1.2	30	57
1336.8-1338	1.12	8	0.5	4.07	3	223.6	0.9	0.52	0.08	11.84	0.89	0.25	5.47	41	3	16.9	1.56	107	91

Table A 2: Methods used to obtain data for Table A1.

Lithium borate fusion, ICP-OES determination				Four acid digests, ICP-OES determination.		Lead collection fire assay 25g charge, ICP-MS determination.	Carbonate fusion, Selective Ion Electrode determination
SiO2	Y	Zr	Eu	S	Nb	Au	F
Fe2O3	Ga	V	Be	Cu	Se	Pd	
CaO	Sn	Sr	Ho	As	Ag	Pt	
Al2O3	U	Ce	Ta	Co	Tl		
K2O	Sc	Cr	Tb	Zn	Bi		
MgO	Sm	Nd	Tm	Ni	Te		
MnO	Pr	W	Lu	Pb	In		
Na2O	Gd	La		Mo	Ge		
P2O5	Hf	Th		Li	Cd		
TiO2	Dy	Rb		Cs	Re		
Ba	Er	Yb		Sb			

ISOTOPES

Table A 3: Complete stable isotope data for samples in SAR8 from GNS Science.

SIL ID	External ID	δD (‰)	$\delta^{18}O$(‰)	Analysis Type	Other Info
G-1701707	8063	-45.5	10.7	D, O18	Calc-silicate/skarn
G-1701708	8075	-68.9	11.9	D, O18	Calc-silicate/skarn
G-1701709	8076	-58.5	12.8	D, O18	Calc-silicate/skarn
G-1701710	8077	-55.1	11.3	D, O18	Calc-silicate/skarn
G-1701711	8078	-62.9	10.7	D, O18	Calc-silicate/skarn
G-1701712	8079	-54.6	12.3	D, O18	Calc-silicate/skarn
G-1701713	8082	-60.3	10.3	D, O18	Calc-silicate/skarn
G-1701714	8083	-59.7	11.8	D, O18	Calc-silicate/skarn
G-1701715	8084	-63.8	9.9	D, O18	Calc-silicate/skarn
G-1701716	8085	-68.8	11.8	D, O18	Calc-silicate/skarn
G-1701717	8086	-74.3	14.1	D, O18	Calc-silicate/skarn
G-1701718	8087	-77.6	11.9	D, O18	Calc-silicate/skarn
G-1701719	8088	-80.1	4.7	D, O18	Calc-silicate/skarn
G-1701720	8089	-69.9	9.9	D, O18	Calc-silicate/skarn
G-1701721	8090	-61.0	11.1	D, O18	Calc-silicate/skarn
G-1701722	8091	-58.8	10.4	D, O18	Calc-silicate/skarn
G-1701723	8093	-55.5	8.5	D, O18	Calc-silicate/skarn
G-1701724	8097	-51.0	8.7	D, O18	Calc-silicate/skarn
G-1701725	8099	-49.6	8.1	D, O18	Calc-silicate/skarn
G-1701726	9000	-58.5	11.2	D, O18	Metasediment

Table A 4: Radiogenic isotope data from SAR8 obtained using methods listed above in: *methods* *(corrected for 152Gd) RAW. ** corrected intensities only.

Serial No.	Sample ID	Function	Mean (After)	2se	Std Dev% (After)	Std Err% (After)	Included	Total	Mean	Std Dev	Std.Dev%	Std.Err%
8851	nw 8063 Sm	147/149 Sm RAW	6.201850	.000528	.0413	.0043	94	100	6.202132	.002961	.0477	.0048
8864	nw 8075 Sm	147/149 Sm RAW	5.078629	.000303	.0294	.0030	97	100	5.078593	.001588	.0313	.0031
8852	nw 8083 Sm	147/149 Sm RAW	5.311244	.000541	.0491	.0051	93	100	5.310844	.003202	.0603	.0060
8853	nw 8085 Sm	147/149 Sm RAW	7.907966	.000378	.0232	.0024	94	100	7.908002	.002221	.0281	.0028
8854	nw 8087 Sm	147/149 Sm RAW	9.893131	.001429	.0711	.0072	97	100	9.893295	.007531	.0761	.0076
8860	nw 8088 Sm RERUN	147/149 Sm RAW	4.130662	.000764	.0887	.0092	92	100	4.130365	.004602	.1114	.0111
8855	nw 8090 Sm	147/149 Sm RAW	6.805934	.000488	.0347	.0036	94	100	6.805944	.002678	.0394	.0039
8856	nw 8091 Sm	147/149 Sm RAW	3.253942	.000189	.0282	.0029	94	100	3.254028	.001081	.0332	.0033
8880	nw 8099 Sm	147/149 Sm RAW	42.862691	.010759	.1197	.0126	91	100	42.854566	.065052	.1518	.0152
8857	nw 9000 Sm	147/149 Sm RAW	5.101751	.000228	.0214	.0022	91	100	5.101629	.001482	.0290	.0029
8850	BHVO-2 87 Sm	147/149 Sm RAW	4.257271	.000583	.0685	.0068	100	100	4.257271	.002915	.0685	.0068

Serial No.	Sample ID	Function	Mean (After)	2se	Std Dev% (After)	Std Err% (After)	Included	Total	Mean	Std Dev	Std.Dev%	Std.Err%
8720	nw 8063 Nd	143/144 Exp	.511705	1.804E-06	.0017	.0002	95	105	.511705	.000011	.0022	.0002
8721	nw 8075 Nd	143/144 Exp	.511716	1.447E-06	.0014	.0001	96	105	.511716	.000009	.0019	.0002
8722	nw 8083 Nd	143/144 Exp	.511058	2.207E-06	.0022	.0002	100	105	.511059	.000012	.0024	.0002
8753	nw 8085 Nd	143/144 Exp	.511583	2.504E-06	.0021	.0002	77	84	.511579	.000024	.0048	.0005
8726	nw 8087 Nd	143/144 Exp	.511387	1.777E-06	.0017	.0002	96	105	.511386	.000011	.0021	.0002
8744	nw 8090 Nd	143/144 Exp	.511740	3.985E-06	.0033	.0004	73	80	.511733	.000030	.0059	.0007
8746	nw 8091 Nd	143/144 Exp	.512967	1.922E-06	.0019	.0002	98	105	.512967	.000013	.0026	.0003
8849	nw 8099 RELOAD Nd	143/144 Exp	.511879	3.443E-06	.0040	.0003	141	161	.511881	.000033	.0064	.0005
8748	nw 9000 Nd	143/144 Exp	.511353	1.664E-06	.0016	.0002	96	105	.511352	.000010	.0020	.0002
8719	BHVO-2 87 Nd	143/144 Exp	.512811	1.494E-04	.1442	.0146	98	105	.512434	.001604	.3131	.0306
8718	JNdi 2017-08-09	143/144 Exp	.512100	.000002	.0021	.0002	98	105	.512100	.000012	.0024	.0002

Serial No.	Sample ID	Function	Mean (After)	2se	Std Dev% (After)	Std Err% (After)	Included	Total	Mean	Std Dev	Std.Dev%	Std.Err%
8851	nw 8063 Sm	152/ 149Sm*	1.839538	0.000188	0.0479	0.0051	88	100	1.840047	0.003239	0.1761	0.0176
8864	nw 8075 Sm	152/ 149Sm	1.919176	0.005335	1.3476	0.139	94	100	1.922666	0.028659	1.4906	0.1491
8852	nw 8083 Sm	152/ 149Sm	1.867655	0.002484	0.6448	0.0665	94	100	1.865887	0.013627	0.7303	0.073
8853	nw 8085 Sm	152/ 149Sm	1.85479	0.00026	0.0691	0.007	97	100	1.854695	0.001373	0.074	0.0074
8854	nw 8087 Sm	152/ 149Sm	1.878596	0.000756	0.2001	0.0201	99	100	1.878514	0.003828	0.2038	0.0204
8860	nw 8088 Sm RERUN	152/ 149Sm	1.895345	0.000436	0.1096	0.0115	91	100	1.895276	0.002665	0.1406	0.0141
8855	nw 8090 Sm	152/ 149Sm	1.875283	0.00056	0.1425	0.0149	91	100	1.875973	0.00338	0.1802	0.018
8856	nw 8091 Sm	152/ 149Sm	1.904573	0.000111	0.0274	0.0029	89	100	1.904637	0.000709	0.0372	0.0037
8880	nw 8099 Sm	152/ 149Sm	1.70029	0.00547	1.5512	0.1608	93	100	1.705004	0.030756	1.8039	0.1804
8857	nw 9000 Sm	152/ 149Sm	1.966979	0.009277	2.3346	0.2358	98	100	1.96894	0.047502	2.4125	0.2413
8850	BHVO-2 87 Sm	152/ 149Sm	1.890131	0.000182	0.0478	0.0048	99	100	1.890149	0.000919	0.0486	0.0049

Serial No.	Sample ID	Function	Mean (After)	2se	Std Dev% (After)	Std Err% (After)	Included	Total	Mean	Std Dev	Std.Dev%	Std.Err%
8720	nw 8063 Nd	150/ 144Nd**	0.568428	0.000241	0.2099	0.0212	98	105	0.568169	0.001511	0.266	0.026
8721	nw 8075 Nd	150/ 144Nd	0.492624	0.000564	0.5867	0.0573	105	105	0.492624	0.00289	0.5867	0.0573
8722	nw 8083 Nd	150/ 144Nd	0.387238	0.000245	0.3245	0.0317	105	105	0.387238	0.001257	0.3245	0.0317
8753	nw 8085 Nd	150/ 144Nd	0.641683	0.000642	0.4418	0.05	78	84	0.641212	0.003223	0.5026	0.0548
8726	nw 8087 Nd	150/ 144Nd	0.654099	0.00081	0.6161	0.0619	99	105	0.654605	0.004426	0.6761	0.066
8744	nw 8090 Nd	150/ 144Nd	0.610473	0.00027	0.1918	0.0222	75	80	0.610229	0.001482	0.2428	0.0271
8746	nw 8091 Nd	150/ 144Nd	0.503628	0.000254	0.2494	0.0252	98	105	0.503404	0.001477	0.2933	0.0286
8849	nw 8099 RELOAD Nd	150/ 144Nd	2.720881	0.003125	0.7285	0.0574	161	161	2.720881	0.019823	0.7285	0.0574
8748	nw 9000 Nd	150/ 144Nd	0.437818	0.000261	0.2936	0.0298	97	105	0.437461	0.001763	0.4029	0.0393
8719	BHVO-2 87 Nd	150/ 144Nd	0.470327	0.000387	0.4052	0.0411	97	105	0.46978	0.002726	0.5802	0.0566
8718	JNdi 2017-08-09	150/ 144Nd	0.238066	0.000251	0.5409	0.0528	105	105	0.238066	0.001288	0.5409	0.0528

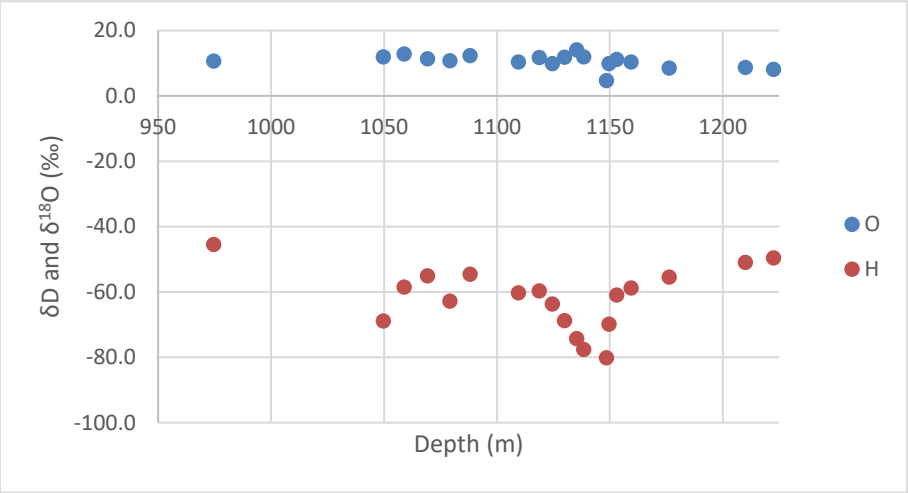

Figure A 3: Isotopic signatures as a function of depth in SAR8.

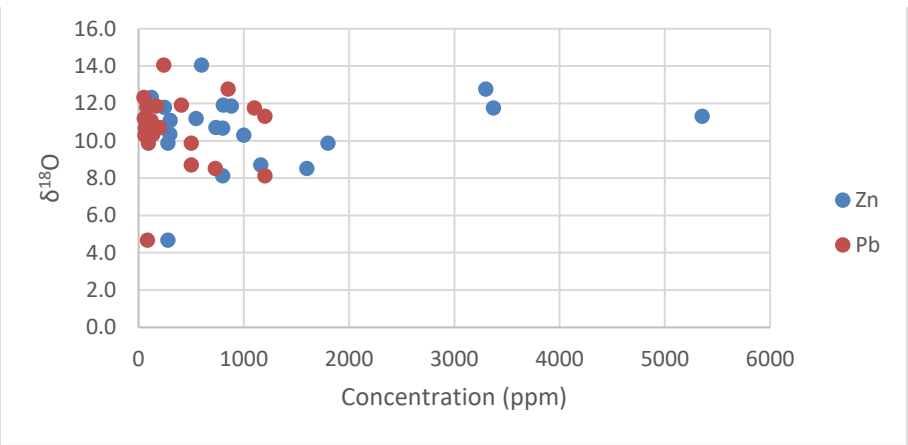

Figure A 4: Relationship between $\delta^{18}O$ and concentration of Zn and Pb.

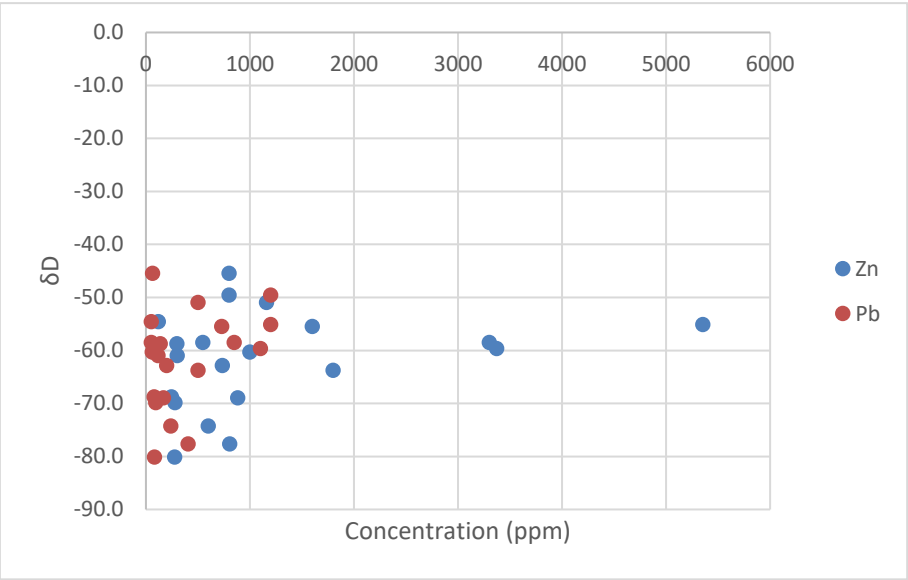

Figure A 5: Relationship between δD and concentration of Zn and Pb.

GARNETS, REE AND TRACE ELEMENTS

Table A 5: LA–ICP–MS data for SAR8.

Sample ID	65	71	77	78	82	83	84	85	86	87	88	89	90	91	93	99
Abundance (ppm)																
Ca	395706.3	136495.2	352244.4	343888.9	311855.2	411842.9	359750	341500	133831.6	322700	410986.7	338157.9	274966.7	418647.1	442323.5	443750
Mg	496.8813	372300	2766.581	21571.18	844.7448	441.5667	566.175	1074.479	112073.7	277.4522	475.6333	3157.484	483.94	1294.088	477.5941	3592.6
Al	19235.5	83504.76	38937.04	36985	53054.14	4963.381	50006.5	28333.82	73289.47	52754.78	25272.47	53294.21	54406	15568.56	56853.53	27106.4
Si	251637.5	932333.3	234959.3	240333.3	236703.4	237295.2	237000	237294.1	1462000	232804.3	312533.3	246157.9	236766.7	243058.8	243858.8	242820
P	73.95	129.4286	213.4815	58	220.2414	69.26667	34.125	81.11765	117.3158	42.01739	97.73333	145.7895	37.73333	82.76471	144	73.25
K	96.93125	7531.714	150.3815	153.0667	763.569	4.128571	15.855	98.42059	29586.32	35.84348	3997.78	594.3684	109.4667	4.5	645.3235	91.65
Sc	12.67288	102.4571	7.421481	18.67917	8.918621	4.351667	28.5265	0.832676	43.29474	14.71913	4.6404	4.691579	11.48	1.280353	35.94059	30.9665
Ti	3766.869	3972.667	2111.037	2086.128	2871	124.9424	7320.05	1101.179	6094.563	4700.87	1624.613	1430.179	5595.8	54.90941	9331.941	671.995
V	238.1338	434.0762	48.48185	61.84611	340.4931	31.22238	257.748	44.55588	133.2105	154.5739	56.058	59.38042	133.6467	51.56294	789.6529	470.51
Cr	35.21438	99.80476	33.96074	13.38722	66.59241	0.129524	138.898	3.313529	104.8842	12.52391	14.966	22.92684	19.9	0.872941	231.0488	21.345
Mn	6233.938	18097.14	8240	6370	7032.069	4348.905	7832	5629.471	29444.74	8282.609	6419.533	8089.526	8765.333	6163.059	8353.588	6170.75
Fe	274731.3	253947.6	229144.4	238777.8	211479.3	303166.7	208250	251676.5	569315.8	207426.1	266633.3	227842.1	215253.3	279823.5	191641.2	263135
Co	1.628875	150.581	59.33004	2.479944	1.957655	0.445571	1.46985	1.136382	109.5789	1.163696	3.498667	19.84211	0.754133	2.212353	1.529235	2.37
Ni	0.260688	400.9048	6.268148	4.051111	1.915862	0.786571	0.28445	2.624706	49.03684	0.386304	0.735267	5.893158	0.243333	3.937647	1.048824	4.821
Cu	2.68	4.496667	1.609889	1.456111	0.467345	0.009095	0.3145	0.186471	7.181053	0.402609	0.512067	1.977895	0.373333	1.746471	0.636706	0.87485
Zn	12.4575	596.0952	21.09	43.96333	8.006552	1.588095	5.7435	8.38	319.8947	3.111304	13.08533	22.20053	3.604	14.04176	8.161765	32.5705
Ga (69)	55.41875	60.15714	19.2937	23.51667	96.90345	70.54286	36.9185	44.06941	47.3	40.96957	17.706	23.53263	44.55333	41.95647	48.2	53.086
Ga (71)	60.6	56.37619	20.03222	24.15	92.03448	71.28095	37.124	44.56882	43.63789	42.18261	16.61067	23.58526	45.97333	42.87059	48.43529	53.636
As	298.1719	11.22857	1025.015	294.9278	115.3097	208.8248	79.066	396.2176	6.5	1.916957	459.1267	263.4579	2.396	492.7647	6.181765	507.92
Se	2.50375	0	0.62037	1.731667	3.038621	2.975714	1.302	1.953235	0.121053	1.709565	0.295333	0.556842	0.913333	2.137059	2.987059	0.986
Y	43.28188	53.30381	20.14407	199.1317	92.44448	72.09662	65.471	40.43824	6.924211	46.55261	20.44707	45.09868	52.30267	24.65942	109.9629	44.587
Zr	74.8575	63.3619	46.79852	60.03772	98.29138	2.050714	143.6325	23.76294	255.9526	99.01391	42.47	59.26826	68.66667	3.513294	107.4353	14.03385
Nb	26.2705	9.182857	9.12963	9.852389	32.23345	1.747581	35.2045	13.04721	33.16095	76.99565	6.487573	7.117432	68.30667	0.807324	49.62706	3.49475
Mo	1.44075	0.236619	1.354333	0.872389	0.512931	0.319476	0.3565	1.021765	0.826053	0.130348	1.738	1.121211	0.102467	1.401941	0.180353	0.2474

Ag	0.01375	0.01	0.168111	0.045222	0.010276	0	0	0.010265	0.108579	0	0.0126	0.059	0.022733	0.002	0.014294	0.0045
Sn	200.1913	12.81095	32.66222	11.11	49.8	176.1762	36.0945	40.83588	9.928421	41.78261	13.35	20.62368	59.03333	31.22941	25.25294	104.105
Sb	0.289313	5.632381	11.20519	0.403556	0.936276	0.047905	0.2499	0.948971	7.774211	0.082748	1.9562	1.349947	0.020733	0.264471	0.360706	0.34225
La	66.90575	0.345429	17.43926	3.188333	6.11469	3.043571	7.12938	11.14788	35.28158	0.109939	56.36533	19.13668	0.068793	12.54724	0.479647	4.2482
Ce	432.1138	1.981714	72.35074	26.22556	49.63931	40.59095	33.56475	84.24265	66.19737	2.927435	254.5667	90.62158	1.448933	97.72471	6.526882	15.71455
Pr	78.39313	0.510143	12.3537	7.157222	14.30138	14.69286	7.28615	19.75353	7.130474	1.744565	38.562	15.42105	0.912333	22.93941	3.339706	3.83285
Nd	305.3625	3.888095	52.74741	46.28167	110.0562	110.6662	50.034	111.7647	23.44316	24.75522	124.58	65.19526	13.908	123.6176	42	26.6505
Sm	26.88188	2.68619	6.787407	20.52	43.14483	31.78762	19.9045	27.31265	2.523053	19.97696	6.750667	9.996842	16.03067	27.94235	32.76412	11.4435
Eu	10.45688	0.686286	7.638889	7.414444	9.351034	18.34762	4.871	10.95471	0.376526	4.005217	6.195333	6.740526	3.824667	10.86176	5.922765	8.8065
Gd	11.12375	4.945238	3.473704	33.80056	29.38172	26.28762	17.1155	16.42912	1.223789	19.82217	3.194	7.937895	24.08333	17.19365	30.36059	12.4585
Tb	1.156375	1.091286	0.422889	6.450944	3.093621	3.452095	2.18545	1.791382	0.191421	2.016391	0.460867	1.144342	3.044867	1.727435	3.886941	1.70225
Dy	7.43475	8.160952	2.955556	39.52128	17.1131	16.83419	12.3275	8.955471	1.035684	10.04565	3.241533	7.053368	14.252	7.235353	21.72353	9.2258
Ho	1.590725	1.792762	0.647519	6.729111	3.259448	2.4903	2.32555	1.504176	0.251632	1.700087	0.7056	1.373979	1.9308	0.944771	4.053176	1.63705
Er	5.0675	5.671429	2.149889	16.42017	9.95069	5.336476	6.7554	3.848265	0.828737	4.486522	2.1704	3.915263	4.273333	1.842682	11.93765	4.42905
Tm	0.740244	0.76981	0.301756	1.986311	1.375931	0.587586	0.93405	0.476971	0.138721	0.577913	0.286073	0.5134	0.473667	0.172276	1.692824	0.59085
Yb	5.199688	5.283333	2.041259	10.98317	9.333793	3.466905	6.463	2.957441	1.120421	3.786522	1.862733	3.293789	3.031333	0.834471	12.23176	3.862
Lu	0.792125	0.768143	0.273415	1.43075	1.195759	0.474576	0.96935	0.386265	0.227316	0.519478	0.237953	0.446668	0.400867	0.079012	1.865882	0.56215
Hf	3.603625	2.433333	1.54537	2.224556	3.192345	0.045857	7.1968	0.809647	7.930526	0.186957	1.381133	2.034316	2.502667	0.064	6.489059	0.60445
W	507.4713	0.262571	461.7259	391.6911	168.0034	265.5952	89.3335	305.1206	3.023421	0.100826	684.2	351.2316	0.175067	430.6353	1.965882	281.7255
Au	0	0	0.019759	0.000922	0.002793	0	0	0.000618	0.005	0.002696	0	0.005211	0.001133	0	0	0
Pb (206)	121.1506	2.426667	148.6815	63.02833	39.38276	47.56667	24.2605	67.55118	10.96526	5.77087	119.8067	82.57368	4.486	80.34118	12.45118	44.7805
Pb (207)	14.27875	0.987143	47.60111	17.87611	7.485517	5.200048	2.87605	7.422647	5.700526	2.269913	14.01467	13.65737	0.802533	12.85706	6.955294	9.011
Pb (208)	1.456313	2.878571	35.59333	13.16033	5.341724	0.445476	0.35645	0.779647	5.676316	2.208826	2.273	5.884368	0.357333	5.623471	6.523765	4.8734
Th	0.737	8.804286	5.25763	2.324167	10.67	2.147905	0.34445	3.914441	8.987368	0.084348	7.394667	1.734526	0.088333	6.258271	2.157765	2.6636
U	107.5819	0.97581	96.48148	44.05222	31.04207	40.06571	21.135	58.28382	12.07947	2.796087	101.9467	67.38895	3.568667	67.27529	5.545294	35.166

Table A 6: McDonough & Sun (1995) values to which SAR8 LA–ICP–MS data was normalised.

La	0.237
Ce	0.613
Pr	0.0928
Nd	0.457
Sm	0.148
Eu	0.0563
Gd	0.199
Tb	0.0361
Dy	0.246
Y	1.57
Ho	0.0546
Er	0.16
Tm	0.0247
Yb	0.161
Lu	0.0246

Elements monitored: *Ag, Al, As, Au, Ca, Ce, Co, Cr, Cu, Dy, Er, Eu, Fe, Ga, Gd, Hf, Ho, K, La, Lu, Mg, Mn, Mo, Nb, Nd, Ni, P, Pb, Pr, Sb, Sc, Se, Si, Sm, Sn, Tb, Th, Ti, Tm, U, V, W, Y, Zn, Zr.*
Isotopes monitored: Pb^{206}, Pb^{207}, Pb^{208}.
The laser as mentioned above in methods operated at a fluence of 11J/cm^2 and at a pulse rate of 5Hz at 65% power level. The spot sizes were 40µm diameter for samples and 50µm for calibration on reference materials. Each spot was sampled over 90 seconds, including background measurements. All LA–ICP–MS data was normalised according to McDonough & Sun (1995) as seen in Table A6.

Table A 7: EMPA data for SAR8.

	65 Core/Light	*65 Rim/Dark*	*77 Core/Light*	*77 Rim/Dark*	*78 Core/Light*	*78 Rim/Dark*	*79 Light*	*83 Light*	*83 Dark*	*84 Core*	*84 Rim*	*85 Core/Dark*	*85 Rim/Light*	*86 Core/Light*	*86 Dark/Rim*
CaO	32.2	32.6	32.25	33.79	32.72	33.89	33.84	32.42	32.55	33.11	32.41	32.36	32.47	33.57	33.47
MgO	0.03	0.05	0.02	0.02	0.08	0.08		0.06	0.02	0.04		0.07	0.09	0.07	0.07
TiO2	0.09	1.09		0.05		0.3	0.41	0.02	0.21	0.7	0.29		0.04	0.44	1.25
SiO2	35.61	36.4	34.76	36.08	35.17	35.49	35.12	35.41	36.97	35.77	35.54	34.44	34.79	35.5	35.55
Al2O3	1.41	5.53		9.32	0.04	8.64	8.9		5.28	6.94	6.95	0.3	1.08	8.36	9.07
Fe2O3	29.42	22.08	31.31	19.35	30.61	19.08	18.99	31.06	24.04	21.91	22.22	29.74	28.55	20.37	17.25
MnO	0.48	0.64	0.55	0.77	0.4	0.74	0.69	0.35	0.69	0.7	0.86	0.4	0.39	0.7	0.75
Cr2O3		0.05													0.1
Cl	0.02	0.02									0.03				
F	0.22	0.1	0.09	0.62		0.8	0.88		0.07	0.15	0.2	0.13	0.14	1.03	0.38
K2O	0.06	0.1							0.03		0.03				0.02
P2O5	0.05	0.05	0.03	0.03	0.03	0.03	0.04		0.03	0.03	0.06	0.03	0.03	0.04	0.04
Na2O	0.07	0.11								0.05	0.09				0.05
BaO											0.03			0.04	
V2O3		0.1		0.05		0.04								0.08	0.19
ZnO		0.07										0.07			
TOTAL	**99.57**	**98.94**	**99.04**	**99.87**	**99.13**	**98.79**	**98.57**	**99.42**	**99.93**	**99.42**	**98.66**	**97.49**	**97.57**	**99.8**	**98.08**

Formulae															
$(Ca,Mg,Mn)_6(Fe,Al)_4Si_6O_{24}$															
Mg	0.009	0.013	0.005	0.005	0.017	0.018	0	0.014	0.005	0.011	0	0.015	0.022	0.016	0.016
Mn	0.069	0.089	0.074	0.102	0.051	0.098	0.092	0.045	0.092	0.094	0.128	0.052	0.049	0.099	0.109
Ca	5.963	5.915	6.011	5.75	5.874	5.771	6.012	5.895	5.799	5.965	5.9	5.963	5.746	5.937	5.752
Total	**6.041**	**6.017**	**6.09**	**5.857**	**5.942**	**5.887**	**6.104**	**5.954**	**5.896**	**6.07**	**6.028**	**6.03**	**5.817**	**6.052**	**5.877**
Fe	3.845	2.798	4.162	2.417	3.911	2.325	2.311	4.019	3.154	2.756	2.806	3.888	3.674	2.522	2.117
Al	0.326	1.265		1.879	0.008	1.368	1.51		1.165	1.399	1.436	0.021	0.273	1.513	1.6
Ti	0.012	0.129		0.007		0.036	0.052	0.003	0.025	0.085	0.038		0.006	0.045	0.136
Cr		0.005													0.001
Total	**4.183**	**4.197**	**4.162**	**4.303**	**3.919**	**3.729**	**3.873**	**4.022**	**4.344**	**4.24**	**4.28**	**3.909**	**3.953**	**4.08**	**3.854**
Si	5.878	5.94	5.973	5.928	5.913	5.888	5.945	5.986	5.896	5.882	5.89	5.959	5.974	5.812	5.865
Al	0.122	0.06	0.027	0.072	0.087	0.112	0.055	0.014	0.104	0.118	0.11	0.041	0.026	0.188	0.135
Total	**6**	**6**	**6**	**6**	**6**	**6**	**6**	**6**	**6**	**6**	**6**	**6**	**6**	**6**	**6**
Total	***16.224***	***16.214***	***16.252***	***16.16***	***15.861***	***15.616***	***15.977***	***15.976***	***16.24***	***16.31***	***16.308***	***15.939***	***15.77***	***16.132***	***15.731***
Spessartine	1.1	1.5	1.4	1.8	1	1.8	1.7	0.8	1.6	1.6	2	1	0.96	1.66	1.74
Grossular	6.4	26.4	0.1	39.5	0.5	38	38.6	0.3	23.8	30.5	30.1	1.6	5.37	35.96	41.81
Andradite	92.5	72	98.5	58.7	98.5	60.2	59.7	98.9	74.7	67.9	67.9	97.4	93.67	62.38	56.15

	87 Core/Light	*87 Rim/Dark*	*89 Core/Dark*	*89 Rim/Light*	*90 Core*	*90 Rim*	*91 Core/Light*	*91 Rim/Dark*	*93 Core*	*93 Rim*	*99 Core/Light*	*99 Rim/Dark*
CaO	32.08	32.96	33.5	32.2	32.4	32.54	32.42	33.77	33.79	33.26	32.93	32.24
MgO	0.08	0.05	0.03		0.06	0.05	0.1	0.08	0.06	0.04	0.05	0.07
TiO2	0.02	1.32		0.02	0.26	0.02	0.03	0.19	1.71	1		
SiO2	34.44	36.53	36.54	35.53	35.13	36.92	34.36	36.06	35.62	35.3	34.81	34.51
Al2O3	1.33	6.54	8.23		7.04	7.62	0.49	9.09	7.95	6.63	3.06	0.2
Fe2O3	28.21	22.41	19.77	30.9	21.5	20.75	30.12	19.01	18.75	21.99	27.13	30.14
MnO	0.6	0.74	0.75	0.55	0.65	0.7	0.45	0.77	0.82	0.69	0.55	0.52
Cr2O3												
Cl	0.03				0.03	0.02	0.02			0.02		
F	0.31	0.16	0.49	0.11	0.81	0.63	0.08	0.74	0.29	0.16	0.12	0.11
K2O	0.02	0.03			0.05	0.03	0.04	0.02		0.01		
P2O5	0.05	0.05		0.04	0.07	0.07		0.02	0.03			0.04
Na2O	0.06	0.06			0.08	0.07	0.05					0.04
BaO							0.03					
V2O3		0.06				0.03		0.16	0.22			
ZnO												0.07
TOTAL	**97.13**	**100.92**	**99.18**	**99.36**	**97.75**	**99.21**	**98.22**	**99.64**	**99.21**	**99.09**	**98.67**	**97.93**

Formulae												
$(Ca,Mg,Mn)_6(Fe,Al)_4Si_6O_{24}$												
Mg	0.018	0.013	0.009	0	0.014	0.013	0.024	0.021	0.014	0.011	0.014	0.016
Mn	0.086	0.107	0.108	0.076	0.091	0.099	0.056	0.112	0.118	0.099	0.08	0.075
Ca	5.772	5.958	6.004	5.914	5.765	5.974	5.897	5.901	5.87	5.903	5.998	5.74
Total	**5.876**	**6.078**	**6.121**	**5.99**	**5.87**	**6.086**	**5.977**	**6.034**	**6.002**	**6.013**	**6.092**	**5.831**
Fe	3.651	2.86	2.458	3.914	2.621	2.587	3.808	2.355	2.327	2.785	3.344	3.801
Al	0.299	1.402	1.456		1.421	1.481	0.189	1.63	1.498	1.123	0.516	0.005
Ti	0.004	0.152		0.003	0.034	0.004	0.004	0.027	0.174	0.12		
Cr												
Total	**3.954**	**4.414**	**3.914**	**3.917**	**4.076**	**4.072**	**4.001**	**4.012**	**3.999**	**4.028**	**3.86**	**3.806**
Si	5.913	5.85	5.874	5.936	5.9	5.876	5.967	5.869	5.834	5.852	5.921	5.915
Al	0.087	0.15	0.126	0.064	0.1	0.124	0.033	0.131	0.166	0.148	0.079	0.085
Total	**6**	**6**	**6**	**6**	**6**	**6**	**6**	**6**	**6**	**6**	**6**	**6**
Total	***15.83***	***16.492***	***16.035***	***15.907***	***15.946***	***16.158***	***15.978***	***16.046***	***16.001***	***16.041***	***15.952***	***15.637***
Spessartine	1.48	1.68	1.74	1.32	1.56	1.6	1.11	1.79	1.87	1.62	1.34	1.27
Grossular	6.45	29.3	36.42		31.25	34.21	2.66	39.48	36.81	29.41	13.61	1.2
Andradite	92.07	69.02	61.84	98.68	67.19	64.19	96.23	58.73	61.32	68.97	85.06	97.53